Parameterization of plume chemistry into large-scale atmospheric models: Application to aircraft NO x emissions

D. Cariolle, D. Caro, R. Paoli, D. Hauglustaine, B. Cuénot, A. Cozic, R. Paugam

Parameterization of plume chemistry into large-scale atmospheric models: Application to aircraft NO_x emissions

D. Cariolle,[1,2] D. Caro,[3] R. Paoli,[1] D. A. Hauglustaine,[3] B. Cuénot,[1] A. Cozic,[3] and R. Paugam[1]

Received 8 February 2009; revised 30 June 2009; accepted 10 July 2009; published 6 October 2009.

[1] A method is presented to parameterize the impact of the nonlinear chemical reactions occurring in the plume generated by concentrated NO_x sources into large-scale models. The resulting plume parameterization is implemented into global models and used to evaluate the impact of aircraft emissions on the atmospheric chemistry. Compared to previous approaches that rely on corrected emissions or corrective factors to account for the nonlinear chemical effects, the present parameterization is based on the representation of the plume effects via a fuel tracer and a characteristic lifetime during which the nonlinear interactions between species are important and operate via rates of conversion for the NO_x species and an effective reaction rates for O_3. The implementation of this parameterization insures mass conservation and allows the transport of emissions at high concentrations in plume form by the model dynamics. Results from the model simulations of the impact on atmospheric ozone of aircraft NO_x emissions are in rather good agreement with previous work. It is found that ozone production is decreased by 10 to 25% in the Northern Hemisphere with the largest effects in the north Atlantic flight corridor when the plume effects on the global-scale chemistry are taken into account. These figures are consistent with evaluations made with corrected emissions, but regional differences are noticeable owing to the possibility offered by this parameterization to transport emitted species in plume form prior to their dilution at large scale. This method could be further improved to make the parameters used by the parameterization function of the local temperature, humidity and turbulence properties diagnosed by the large-scale model. Further extensions of the method can also be considered to account for multistep dilution regimes during the plume dissipation. Furthermore, the present parameterization can be adapted to other types of point-source NO_x emissions that have to be introduced in large-scale models, such as ship exhausts, provided that the plume life cycle, the type of emissions, and the major reactions involved in the nonlinear chemical systems can be determined with sufficient accuracy.

Citation: Cariolle, D., D. Caro, R. Paoli, D. A. Hauglustaine, B. Cuénot, A. Cozic, and R. Paugam (2009), Parameterization of plume chemistry into large-scale atmospheric models: Application to aircraft NO_x emissions, *J. Geophys. Res.*, *114*, D19302, doi:10.1029/2009JD011873.

1. Introduction

[2] The emission of gaseous and particulate exhausts from aircraft engines can locally raise the atmospheric species concentrations by several orders of magnitude. If the exhausts are chemically reactive, they can induce strong local perturbations in the chemical composition that persist over a long time after complete dilution of the plume. The nonlinear character of the photochemical systems is at the origin of these disturbances. Indeed, the rates of production and loss of the species are computed as the product of concentrations, so one can obtain rapid evolutions in the concentration of the species within the plumes and during their dispersion.

[3] The resolution of the large-scale models does not account for this transient phase where the plume size is smaller than the global-model grid size. Most of the time the emissions by local sources are considered as instantaneously mixed at the smallest resolved scale. In this way, the nonlinear chemical processes are neglected, and significant errors can be introduced in the emission rates of primary compounds and on the level of the secondary products in the computational cells containing exhaust plumes. In the specific case of aircraft emissions that is considered hereafter, the emissions of nitrogen oxides, sulphate aerosols and soot particles lead to large local variations in the

[1]Centre Européen de Recherche et de Formation Avancée en Calcul Scientifique, URA1875, CNRS, Toulouse, France.
[2]Météo-France, Toulouse, France.
[3]Laboratoire des Sciences du Climat et de l'Environnement, CEA, Gif-sur-Yvette, France.

0148-0227/09/2009JD011873

concentration of ozone and to conversion of a significant fraction of the nitrogen oxides (NO_x) to nitric acid.

[4] To improve the accuracy of global models, these effects must be taken into account and several methods have been proposed, mainly on the basis of the introduction of corrective factors in the rates of injection of primary or secondary pollutants. For example, *Petry et al.* [1998], *Meijer* [2001], and *Kraabøl et al.* [2002] have developed methodologies to calculate effective emission indices or emission conversion factors that take into account the transition phases in the chemical system during plume dispersion. Their methods are based on coupled chemistry and diffusion-type models to compute the corrective coefficients that have to be introduced into the rates of emitted or produced species. Those factors are species-dependent and vary according to the large-scale background composition of the atmosphere, the latitude, season and the time of injection. They are calculated both for emitted species like the NO_x, and for species produced during the dilution of the plume, for, for example, O_3 and HNO_3. A review of the various approaches followed so far is given by R. Paoli et al. (Modeling and computation of Effective Emission Indices: A position paper, manuscript in preparation, 2009).

[5] These methods were applied to the evaluation of the influence on atmospheric chemistry of the subsonic aircraft traffic, whose major effect is the increase of tropospheric ozone [*Brasseur et al.*, 1996]. In all cases, taking into account corrective factors leads to a reduction of the ozone production by 10 to 20% depending on season and latitude.

[6] Although these methods provided satisfactory and consistent results in term of reduction of ozone production, they present some limitations that we try to overcome in this study. One issue is that mass conservation of the species is difficult to insure, especially for ozone that is a secondary product subjected to the acceleration or deceleration of the catalytic cycles controlling its production or destruction. The ozone emission conversion factors must then depend on those of the species directly emitted. Furthermore, the corrective factors should reflect the conditions for plume dispersion that vary according to the intensity of the atmospheric turbulence. In the various implementations made until now the correcting factors have a climatological character and are precomputed to account for latitudinal and seasonal variations, but do not always account for the local and regional dispersion properties of the atmosphere. In particular the plumes are assumed to dissipate in the vicinity of the emission location, although the dilution process can take several hours, and during that time the emitted species can be advected for several hundred kilometers at the tropopause level.

[7] The objective of the present paper is to present an alternative method to parameterize the nonlinear chemical effects during plume dispersion that cope with some of the issues mentioned above. The method is based on the introduction of an "exhaust or fuel tracer" that traces the fraction of the emissions not yet diluted at large scale. The tracer is used to compute the rates of NO_x and HNO_3 released at the scale of the CTM grid cell, and to determine the effective reaction rates that are responsible for ozone destruction within the plumes.

[8] This paper is organized as follows. Section 2 describes the method and its application to the injection of NO_x by aircraft, the formation of HNO_3 and the induced O_3 evolution. Section 3 details the implementation of our parameterization in the 3D LMDz-INCA and the 2D MOBIDIC chemical transport models (CTM), and the results obtained on the impact of present subsonic aircraft fleet. In section 4 possible improvements of the method and application to other types of source point emissions are discussed. The final section summarizes the results.

2. Description of the Method

[9] In this section the set of model equations that have to be integrated into CTM to take into account transient chemical processes during plume dispersion is presented. Although the present approach can be generalized, the particular case of ozone production/destruction by nitrogen oxides emitted by aircraft at cruise altitude and their conversion into HNO_3 are considered hereafter.

2.1. Basic Formulation

2.1.1. A Plume Model and Its Representation in CTM

[10] During the dilution phase, the species concentrations in the plume can be several orders of magnitude higher than background concentrations, so that a given reaction operating inside the plume may be much more efficient than the same reaction occurring in the background atmosphere. This is due to the fact that the rates of species production/destruction depend on the product of concentrations of the reacting species, and this product depends on the degree of dilution of the plume: it usually gets the highest value just after the emission, then decreases until the species in the plume get sufficiently well mixed with background so that chemical reactions proceed as in the surrounding atmosphere. Such threshold on dilution corresponds to a limiting mixing ratio r_l of an emitted species below which the perturbation of the chemical system can be neglected.

[11] In the case of NO_x emission at cruise altitude the background volume mixing ratios r_b are in the range of 0.007 ppbv (clean air) to 0.15 ppbv (flight corridors), whereas at time t_0 of a few minutes after emission, the mixing ratio for a typical plume generated by a long-range aircraft of the B747 type is about $r_p(t_0) \simeq 20$ ppbv [*Schumann et al.*, 1998]. The analysis of the NO_x/O_3 chemical interactions (section 2.2) shows that the perturbed regime for ozone is maintained for NO_x content up to about 1 ppbv. It is then needed to trace the fraction of the plume where the NO_x mixing ratio r_p is larger than 1 ppbv ($r_p > r_l = 1$ ppbv), and to parameterize its impact on the chemical rates in the large-scale model.

[12] To that end, the plume and the associated high-concentration emissions are represented as the quantity of exhaust material occupying the volume V_p where the mixing ratio is larger than r_l, or equivalently the dilution ratio $r_p/r_p(t_0)$ is between 1 and $r_l/r_p(t_0)$. The complementary fraction of the emissions (with $r < r_l$) is assumed to be released at the model scale and to proceed like if it was well mixed with the background air.

[13] To represent this process at global scale a "fuel tracer" is added to the CTM variables. This tracer gives the quantity of exhaust material highly concentrated within the plume. Assuming that the dilution occurs mainly via diffusion-type processes, the time evolution of the tracer is approximated

by an exponential decay with the characteristic time τ. Denoting by $\overline{r_f}$ the mass mixing ratio of this tracer averaged over the grid cell, its continuity equation reads

$$\frac{\partial \overline{r_f}}{\partial t} + \langle F_f \rangle = I - \frac{1}{\tau}\,\overline{r_f} \tag{1}$$

where $\langle F_f \rangle \equiv \nabla \cdot (\overline{r_f}\mathbf{u}) + \nabla \cdot (D_t \nabla \overline{r_f})$ denotes the divergence of the fluxes associated to large-scale transport (advection and turbulent diffusion) of the tracer, I is the fuel injection rate (proportional to the mass of fuel consumption per unit of time) obtained from emission data, and τ is a decay time.

[14] The determination of τ requires to evaluate the mass of the above-threshold exhaust inside the plume (with $r_p > r_l$) using small-scale modelization or observations,

$$M(t) = \int_{V_p} \rho\, r_p\, dV. \tag{2}$$

As discussed above, during the plume dilution process the mass $M(t)$ decreases continuously until $t = T_l$ beyond which the mixing ratio r_p is everywhere below r_l and $M = 0$. The value of τ is obtained by approximating $M(t)$ by an exponential function whose time integral is the same as the "exact" mass integral,

$$\tau \equiv \int_{t_0=0}^{+\infty} \exp(-t/\tau)\, dt = \frac{1}{M(t_0)} \int_{t_0=0}^{T_l} M(t)\, dt. \tag{3}$$

The value of τ depends on the choice of r_l, on the initial plume characteristics and on the dispersion properties of the atmosphere. In Appendix A, details on the evaluation of τ are given for a simple case where the initial plume is about 250 m wide and the dissipation is assumed to be solely due to horizontal diffusion, modeled using a coefficient typical of what currently derived for the upper atmosphere (D_h = 20 $m^2\ s^{-1}$). In that case the exponential function approximates the $M(t)$ function within 20% for 80% of the mass evolution, with a tendency to underestimate the mass fractions at the beginning of the plume evolution, and to overestimate it toward the end of the dissipation process. In the context of global circulation models this means that the present approach slightly underestimates the plume effects in the corridor regions, but the global fraction of the highly concentrated plume air masses is maintained fully consistent with the one of the detailed plume model.

[15] In reality, the nature of atmospheric turbulence is much more complex than a simple horizontal diffusion. However, since our objective is to model with reasonable accuracy the evolution of the undiluted fraction of the emissions within the grid of a large-scale model, the approximation of this evolution by an exponential function seems adequate and workable within the CTMs framework. The evaluation of the value of τ is further discussed in section 2.4.

[16] Once τ is determined, equation (1) can be integrated and the volume mixing ratio at the large scale of any emitted species in high-concentration plume form is then obtained by multiplying $\overline{r_f}$ by its emission index. For the NO_x(= NO+NO_2) species studied here, one writes

$$\overline{r_{\mathrm{NO_x}^p}} = \overline{r_f}\, \alpha_{\mathrm{NO_x}}\, EI_{\mathrm{NO_x}}, \tag{4}$$

where $\overline{r_{\mathrm{NO_x}^p}}$ is the NO_x volume mixing ratio in the undiluted phase, $EI_{\mathrm{NO_x}}$ is the emission index for the NO_x (in g/kg), and $\alpha_{\mathrm{NO_x}} = 10^{-3}\, M_{\mathrm{air}}/M_{\mathrm{NO_x}}$ where M_{air} and $M_{\mathrm{NO_x}}$ are the molecular mass of the air and of NO_x, respectively.

[17] Through dilution, the NO_x in the high-concentration phase are restored into the background phase noted by $\overline{\mathrm{NO_x}}$ (all overlined quantities refer to CTM grid averages). The mixing ratio of $\overline{\mathrm{NO_x}}$ is thus the solution of the equation

$$\frac{\partial r_{\overline{\mathrm{NO_x}}}}{\partial t} + \left\langle F_{\overline{\mathrm{NO_x}}} \right\rangle = \frac{1}{\tau}\,\overline{r_f}\,\alpha_{\mathrm{NO_x}}\, EI_{\mathrm{NO_x}} + L_{\mathrm{ss}}, \tag{5}$$

where L_{ss} is large-scale chemical sources and sinks.

2.1.2. Determination of Effective Rate Constants

[18] Knowing the fraction of the injected species in the diluted and high-concentration phases, one can compute the rates of production/destruction of the secondary formed/destroyed species. These rates are modified within the plume air masses compared to the background atmosphere because of the higher concentrations of the injected species. As discussed below, the modified rates can be introduced via the determination of effective reaction rate constants K_{eff} which are used to compute secondary formed species within the plume.

[19] For example, let us consider the evolution of species A and B reacting in a volume V of the atmosphere with a constant rate K. The exhaust plume occupies the fraction V_p of the volume V. In the CTM context V represents the volume of a computational cell. At the beginning of the plume evolution the volume V_p increases with the plume expansion, reaches a peak value, and decreases afterward up to time T_l when $M(T_l) = V_p(T_l) = 0$ (see Appendix A).

[20] Thus, the total rate of change R of the concentrations of species A and B over the volume V can be split into background and plume contributions,

$$R = -\frac{1}{V}\int_{V-V_p} K\, C_A\, C_B\, dV - \frac{1}{V}\int_{V_p} K\, C_A\, C_B\, dV, \tag{6}$$

where C_A and C_B are the concentrations of A and B. The last term of the right-hand side of equation (6) is only significant during the lifetime of the plume, i.e., before it gets diluted to background. So we estimate this term as a time average over T_l (with $T_l \gg t_0$) and rewrite R as

$$R = -\frac{1}{V}\int_{V-V_p} K\, C_A\, C_B\, dV - \frac{1}{T_l}\frac{1}{V}\int_{t_0}^{T_l}\int_{V_p} K\, C_A\, C_B\, dV\, dt. \tag{7}$$

We now assume that outside the plume the species are well mixed with background concentrations denoted by $\overline{C_A}$ and $\overline{C_B}$. With this assumption the rate R takes the form

$$R = -\frac{(V - V_p)}{V} K\, \overline{C_A}\, \overline{C_B} - \frac{1}{T_l}\frac{1}{V}\int_{t_0}^{T_l}\int_{V_p} K\, C_A\, C_B\, dV\, dt. \tag{8}$$

We further assume that at any time the volume occupied by the high-concentration fraction of the exhaust will be much smaller than the volume grid, so $V_p \ll V$. Since we have $V_p < r_p(t_0)\, V_p(t_0)/r_p < r_p(t_0)\, V_p(t_0)/r_l = [r_p(t_0)\, V_p(t_0)/(r_l V)]\, V$,

the condition $V_p \ll V$ is fulfilled if the dilution ratio $r_l/r_p(t_0)$ is larger than $V_p(t_0)/V$. In other words, the dilution ratio must be higher than the ratio between the initial volume of the plume and the grid volume. This is clearly the case for the configurations that we treat with our 3D model (section 3) since $r_l/r_p(t_0)$ is about 0.05 whereas $V_p(t_0)/V$ is 0.000083 (for a single plume with an initial cross section of 100 m × 250 m and a model grid of 300 km horizontal and 1 km vertical sizes).

[21] For multiple plumes we have to consider the total volume occupied by the initial plumes in the computational grid, which depends on the density of air traffic, in particular the average number of airplanes present in a grid box during the time T_l. According to *Kärcher and Meilinger* [1998] the average flux density of aircraft is about ϕ = 0.4 d^{-1} km^{-2} (the surface evaluated in the cross section perpendicular to the flight direction) in the dense NAFC. For the 3D CTM configuration used in section 3 it gives about 120 aircraft per day per grid box, whereas more than 500 airplanes should fly over the time T_l within the model grid to approach a value of $r_l/r_p(t_0)$ close to $V_p(t_0)/V$. Consequently the condition $r_l/r_p(t_0) > V_p(t_0)/V$ will be met for the settlings of our CTM, and is even more easily fulfilled in the case of the 2D model simulations (section 3). So, we can assume that $(V - V_p)/V = 1$ and equation (8) reduces to

$$R = -K\,\overline{C_A}\,\overline{C_B} - \frac{1}{T_l}\frac{1}{V}\int_{t_0}^{T_l}\int_{V_p} K\,C_A\,C_B\,dV\,dt. \tag{9}$$

Species A and B have mean plume concentrations

$$C_A^p = \frac{1}{T_l}\frac{1}{\widetilde{V_p}}\int_{t_0}^{T_l}\int_{V_p} C_A\,dV\,dt, \quad C_B^p = \frac{1}{T_l}\frac{1}{\widetilde{V_p}}\int_{t_0}^{T_l}\int_{V_p} C_B\,dV\,dt \tag{10}$$

(with $\widetilde{V_p} = \frac{1}{T_l}\int_{t_0}^{T_l} V_p dt$) that can be very different from the corresponding background values. Inside the plume and over its lifetime T_l the concentrations C_A and C_B vary significantly, so the averaged value of the product $C_A.C_B$ is different from the product of the mean values $C_A^p.C_B^p$. We therefore introduce a "plume" (p) reaction rate constant defined as

$$K^p = \frac{1}{C_A^p\,C_B^p}\frac{1}{T_l}\frac{1}{\widetilde{V_p}}\int_{t_0}^{T_l}\int_{V_p} K\,C_A\,C_B\,dV\,dt. \tag{11}$$

The deviation of K^p from K gives a measure of the impact of the nonlinearity and the nonhomogeneity of the chemical system on the reaction between A and B within the plume. If the system is moderately affected by the injected species and their high concentrations, the value of K^p is close to the value of K. Otherwise during the plume lifetime the segregation effects can be important and the reaction between A and B can proceed at a much different rate than would be inferred using average concentrations. The ratio K^p/K gives an evaluation of the segregation factor, as introduced by *Vila-Guerau de Arellano et al.* [1993] for chemical rates that control the ozone production in turbulent reactive boundary layers.

[22] Using the definition of K^p given by equation (11), the rate of concentration change R is now expressed as

$$R = -K\,\overline{C_A}\,\overline{C_B} - K^p\,C_A^p\,C_B^p\,\frac{\widetilde{V_p}}{V}. \tag{12}$$

In the general case the values of C_A^p and C_B^p cannot be directly determined from the CTM concentrations, and further assumptions have to be made. In our case we treat the situation where some species are injected in large amounts (e.g., NO_x), and others are not injected and preexist in the atmosphere (e.g., O_3). The concentrations of the species injected in the plume can be related to their large-scale concentration by an equation similar to equation (4). So if we assume that species B is emitted, its grid-averaged plume concentration is given by

$$\overline{C_B^p} = \frac{1}{T_l}\frac{1}{V}\int_{t_0}^{T_l}\int_{V_p} C_B\,dV\,dt = \overline{r_f}\,\rho\,\alpha_B\,EI_B \tag{13}$$

and is related to the plume concentration C_B^p by the relation

$$C_B^p = \frac{V}{\widetilde{V_p}}\,\overline{C_B^p} = \frac{V}{\widetilde{V_p}}\,\overline{r_f}\,\rho\,\alpha_B EI_B. \tag{14}$$

Substituting $\overline{C_B^p}$ at place of C_B^p in equation (12) the rate R now takes the form

$$R = -K\,\overline{C_A}\,\overline{C_B} - K^p\,C_A^p\,\overline{C_B^p}. \tag{15}$$

If species A is not injected, its concentration within the plume C_A^p will be function of its background concentration $\overline{C_A}$, and of possible transformations within the plume. Thus, we introduce an "effective" reaction rate constant, K_{eff}, defined as

$$K_{eff} = K^p\,\frac{C_A^p}{\overline{C_A}} \tag{16}$$

$$K_{eff} = \frac{1}{\overline{C_A}}\frac{1}{\overline{C_B^p}}\frac{1}{T_l}\frac{1}{V}\int_{t_0}^{T_l}\int_{V_p} K\,C_A\,C_B\,dV\,dt. \tag{17}$$

Alternatively, using equation (13) K_{eff} can be expressed in the integral form

$$K_{\text{eff}} = \frac{1}{\overline{C_A}}\,\frac{\int_{t_0}^{T_l}\int_{V_p} K\,C_A\,C_B\,dVdt}{\int_{t_0}^{T_l}\int_{V_p} C_B\,dV\,dt}, \tag{18}$$

and the rate R is finally recast as

$$R = -K\,\overline{C_A}\,\overline{C_B} - K_{\text{eff}}\,\overline{C_A}\,\overline{C_B^p}. \tag{19}$$

[23] Provided that K_{eff} can be evaluated, the rate R is now entirely determined by concentrations evaluated at the scale of the model (overlined quantities). This procedure has analogies with "closure" problems in turbulent modeling

where the subgrid-scale fluxes are modeled using quantities defined at the larger resolved scale.

[24] In practice K_{eff} has to be diagnosed from small-scale plume simulations using equation (18). In Appendix A we give a simple example where we derive the values of τ and K_{eff}, but the methodology can be easily applied to any small-scale model, like Gaussian plume models or large-eddy simulations.

[25] In this study we consider the case where K_{eff} is determined to treat the impact of the plume chemistry on the odd oxygen tendencies of our CTMs. In that case species A represents the sum of the odd oxygen species $O_x = O_3 + O + NO_2$. In the background atmosphere $O_3 \gg O$ and $O_3 \gg NO_2$, so we can consider that $O_x = O_3$. Within the plume, with high NO_x content, the calculations detailed in section 2.2 show that the odd oxygen species are dominated by O_3 and NO_2. So $O_x = O_3 + NO_2$, and the O_x evolution is dominated by the NO_x catalytic cycle. Since most of the NO_x is injected in form of NO, the concentrations of O_x inside and outside the plume are identical just after the plume formation, although their rate of change will be afterward different. In that configuration the rate of O_x concentration change due to the plume effects takes the form

$$R = \ldots - K_{\text{eff}}\,\overline{O_x}\,\overline{NO_x^p} \tag{20}$$

where $\overline{O_x}$ and $\overline{NO_x^p}$ denote, respectively, the concentration of O_x and the grid-averaged concentration of the fraction of NO_x in the plume state (given by equation (13) with $EI_B = EI_{NO_x}$ and $\alpha_B = \alpha_{NO_x}$).

[26] Since $V \gg V_p$ the fraction of O_3 transformed into NO_2 inside the plume can be neglected at the scale of the model grid, so we end up for the continuity equation of the ozone mixing ratio $\overline{r_{O_3}}$ with

$$\frac{\partial \overline{r_{O_3}}}{\partial t} + \langle F_{O_3} \rangle = \ldots - K_{\text{eff}}\,\overline{NO_x^p}\,\overline{r_{O_3}} + \ldots \tag{21}$$

where K_{eff} is the effective reaction rate constant for the ozone reaction with the fraction of the NO_x in the highly concentrated plume form. This reaction then adds to the large-scale reactions for background concentrations.

[27] In the authors' opinion, the proposed method presents a number of advantages over the methods which use emission conversion factors for O_3, such as those of *Petry et al.* [1998] and *Meijer* [2001]. First, the system formed by equations (1), (4), (5) and (21) is fully conservative for the injected species, and relaxes to standard large-scale formulation (i.e., without plume) when $\tau \to 0$, i.e., for "instantaneous" dilution. In that case $\overline{r_f} \to I\tau$ and the term $\frac{1}{\tau}\overline{r_f}\,\alpha_{NO_x} EI_{NO_x} \to I\alpha_{NO_x} EI_{NO_x}$ in equation (5).

[28] Another advantage of the proposed method is that in the case of secondary formed species like O_3, the introduction of effective reaction rates does not directly introduce precomputed tendencies in equation (21), but act as a modulation of the chemical cycles existing in the background atmosphere. In the case of instantaneous dilution the right-end side term of equation (21) disappears because $\overline{r_f}$, $\overline{r_{NO_x^p}}$ and $\overline{NO_x^p} \to 0$ when $\tau \to 0$, and only the terms from the large-scale chemical sources and sinks remain in the equation.

[29] Finally, since the method takes into account the transport of pollutants during the plume dilution, the nonlinear chemical effects can apply rather far from the point of injection depending on the large-scale advection and the plume lifetime. This is a clearly advantage over the use of conversion factors that are applied instantaneously at injection.

[30] The key point is the determination of τ and K_{eff} for ozone. *Meijer* [2001] uses a Gaussian diffusion model to model the dispersion of the aircraft plumes and to compute the conversion factors. This approach or even more sophisticated models [see, e.g., *Lewellen and Lewellen* [2001] for the analysis of far-field evolution of aircraft wakes) may be used to derive the plume lifetime τ and the effective reaction rates K_{eff}. It would require to diagnose the evolution of the mass of exhaust $M(t)$ (equation (2)), and the integrals of equation (18) during the course of the integration.

[31] In this work, simplified approaches are used, based on a box chemical and 1D models to evaluate the K_{eff} for the ozone destruction within the plumes, and on a constant lifetime τ inferred from model calculations based on current estimates of the mean dispersion properties of the atmosphere at the midlatitude tropopause level. The methodology and the choices made for the implementation are detailed in section 2.2, 2.3, and 2.4.

2.2. Ozone Destruction/Production Rate With High NO_x Concentrations

[32] In the troposphere and lower stratosphere, the increase of nitrogen oxides at moderate level leads to the production of O_3 via the oxidation of hydrocarbons [*Crutzen*, 1974]. The key chemical cycle involves the conversion of nitric oxide into nitrogen dioxide by peroxy radicals (RO_2),

$$NO + RO_2 \longrightarrow NO_2 + RO, \tag{R1}$$

followed by photolysis of NO_2 and recombination of atomic oxygen with molecular oxygen to form O_3 (reactions (R2) and (R3) below). As a consequence the NO_x emissions by tropospheric sources, like aircraft, leads to large-scale O_3 production [e.g., *Brasseur et al.*, 1996].

[33] The situation is very different if large amount of NO_x is injected so that its concentration may be on the same order as the O_3 concentration. This is typically the case with the plume formed behind aircraft or close to any source of combustion ground level. In that case the ozone evolution depends on the following five main reactions:

$$NO_2 + h\nu \longrightarrow NO + O, \tag{R2}$$

$$NO + O_3 \longrightarrow NO_2 + O_2, \tag{R3}$$

$$O + O_2 \longrightarrow O_3, \tag{R4}$$

$$O + NO_2 \longrightarrow NO + O_2, \tag{R5}$$

$$O + O_3 \longrightarrow 2O_2. \tag{R6}$$

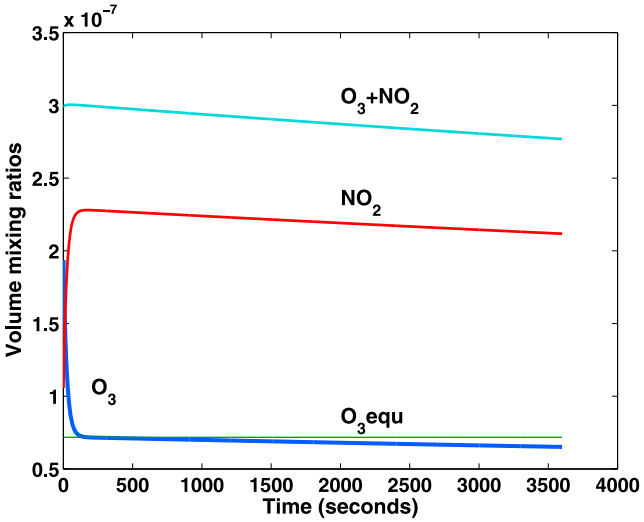

Figure 1. Evolution of the mixing ratios of NO_x and O_3 after injection of 1 ppmv of NO_x at 200 hPa (initial conditions for the simulation: 0.2 ppmv for O_3 and T = 230 K). The O_3 concentration (blue line) decreases rapidly owing to titration by NO_2. The odd oxygen species (O_3+NO_2) show a slower continuous decrease.

Using the conservation equations for each reacting species of the above system, one obtains for the evolution of the sums of the concentrations,

$$d(\mathrm{O}+\mathrm{O_3})/dt = +k_2\cdot\mathrm{NO_2} - k_3\cdot\mathrm{NO}\cdot\mathrm{O_3} - k_5\cdot\mathrm{O}\cdot\mathrm{NO_2} - 2\cdot k_6\cdot\mathrm{O_3}\cdot\mathrm{O} \tag{22}$$

$$d(\mathrm{O}+\mathrm{O_3}+\mathrm{NO_2})/dt = -2\cdot k_5\cdot\mathrm{O}\cdot\mathrm{NO_2} - 2\cdot k_6\cdot\mathrm{O_3}\cdot\mathrm{O} \tag{23}$$

$$d(\mathrm{NO}+\mathrm{NO_2})/dt = 0, \tag{24}$$

where k_i is the rate constant of reaction (R1). From equations (22)–(24), one can identify two regimes controlling the daytime chemical system when nitrogen oxides are injected in large quantities.

2.2.1. Regime I

[34] The first chemical regime is characterized by the rapid equilibrium between NO and NO_2 that is reached via reactions (R2) and (R3) in a few minutes. At the end of this regime, NO, NO_2 and O_3 have equilibrium concentrations that can be approximated with good accuracy by

$$\mathrm{NO_2}/\mathrm{NO} = k_3/k_2\,\mathrm{O_3^{equ}} \tag{25}$$

$$\mathrm{O_3^{equ}} = -1/2\left(k_2/k_3 + \mathrm{NO_x} - O_3^i\right) + \sqrt{1/4\left(k_2/k_3 + \mathrm{NO_x} - O_3^i\right)^2 + k_2/k_3\,O_3^i}, \tag{26}$$

where O_3^i is the initial ozone concentration. Figure 1 shows the evolution of species mixing ratios in a typical simulation obtained with a comprehensive photochemical box model (that includes the system of reactions (R2)–(R6), as well as HO_x, NO_y, Cl_x reactions for the ozone budget and the methane oxidation chain) in the case of NO_x injection in the upper troposphere. In this case (injection of 90% of NO and 10% of NO_2), the equilibrium is reached very quickly, and a large fraction of O_3 is converted into NO_2 via the reaction (R3).

[35] Ozone is thus stored in the form of NO_2 and can be released later after dilution, depending on the relative balance between $\overline{\mathrm{NO}}$ and $\overline{\mathrm{NO_2}}$ in the diluted phase at the large scale. As a consequence, the associated effect of this regime on the ozone budget can be written as

$$\frac{\partial\overline{r_{\mathrm{O_3}}}}{\partial t} + \langle F_{\mathrm{O_3}}\rangle = .. - \frac{1}{\tau}\,\overline{r_f}\,\alpha_{\mathrm{NO_x}}\,EI_{\mathrm{NO_x}}\left(\overline{\mathrm{NO_2}}/\overline{\mathrm{NO_x}} - \mathrm{E}\right)\delta\ldots \tag{27}$$

with δ being equal to 1 (0) for daytime (nighttime) conditions, and E being the ratio equal to the proportion of NO_2 in the NO_x initial emissions. If the background atmospheric ratio $\overline{\mathrm{NO_2}}/\overline{\mathrm{NO_x}}$ is higher (lower) than the initial E, ozone is destroyed (produced). Generally, for most of the NO_x aircraft sources, the value of E lies between 0 and 0.1, whereas in the free atmosphere the ratio $\overline{\mathrm{NO_2}}/\overline{\mathrm{NO_x}}$ is between 0.3 and 0.6 in the upper troposphere. So in most cases, NO_x injection leads to ozone destruction. This destruction will be however quite limited since it does not correspond to a catalytic cycle but to a titration effect, and the ozone loss rate will be at most equal to the NO_x injection rate.

2.2.2. Regime II

[36] Just after completion of the regime I, the system enters into a second regime where the ozone evolution is driven by equation (23). The full calculation with the chemical model shows that $O_3 \gg O$ and that $k_5\cdot\mathrm{NO_2} \gg k_6\cdot\mathrm{O_3}$. Equation (23) may then be reduced to

$$d(\mathrm{O_3}+\mathrm{NO_2})/\mathrm{dt} = -2\cdot\mathrm{k_5}\cdot\mathrm{O}\cdot\mathrm{NO_2}. \tag{28}$$

Using our box model the K_{eff} coefficient associated to this reaction is evaluated using equations (11) and (16) with $C_A^p \simeq \overline{C_A} = \mathrm{O_x}$ and $C_B^p = \mathrm{NO_x}$. Averaged over the time T the value of K_{eff} is given by

$$K_{\mathrm{eff}} = 2\left(\int^T k_5\,\mathrm{O}\cdot\mathrm{NO_2}\,dt\right)\Big/\left(\mathrm{NO_x}\int^T \mathrm{O_x}\,dt\right). \tag{29}$$

For NO_x concentrations above 1 ppbv the time evolution of the O_x concentration calculated with the box model with full chemistry was found similar to the evolution diagnose using equation (28) alone. The ozone production via (R1) was not found significant compared to the odd oxygen destruction via (R5). Then, most of the ozone production occurs for NO_x content lower than 1 ppbv within the "diluted" fraction of the emission at a rate close to what is calculated at the CTM scale.

[37] Finally, taking into account the two regimes described above, the ozone continuity equation (see equation (21)) becomes

$$\frac{\partial\overline{r_{\mathrm{O_3}}}}{\partial t} + \langle F_{\mathrm{O_3}}\rangle = \ldots - \frac{1}{\tau}\,\overline{r_f}\,\alpha_{NO_x}\,EI_{\mathrm{NO_x}}\left(\overline{\mathrm{NO_2}}/\overline{\mathrm{NO_x}} - E\right)\delta - K_{\mathrm{eff}}\,\overline{r_f}\,\rho\,EI_{\mathrm{NO_x}}\,\overline{r_{\mathrm{O_3}}}\,\delta + \ldots \tag{30}$$

that can be recast as

$$\frac{\partial \overline{r_{O_3}}}{\partial t} + \langle F_{O_3} \rangle = \ldots - \left[\frac{1}{\tau} \left(\overline{NO_2}/\overline{NO_x} - E \right) + K_{eff}\, \overline{r_{O_3}}\, \rho \right] \cdot \overline{r_f}\, \alpha_{NO_x}\, EI_{NO_x}\, \delta + \ldots . \quad (31)$$

[38] The present approach differs from those that use emission conversion factors and introduce a net production O_3 rate per injected NO_x species. The major difficulty of the conversion factor methods is to avoid the double counting of ozone production. Indeed, two ozone sources/sinks are introduced by these methods, one direct through the use of a conversion factor for ozone, the other via the increase of the NO_x content at the resolved CTM scale. The first source must be carefully evaluated as additional to the second one, but this cannot be easily achieved by precalculating ozone tendencies in conditions that do not exactly match the CTM state. Our approach avoids this difficulty by performing a net separation between the calculation of the ozone tendencies due to the chemical processes at the model scale and the ozone tendencies due to the plume chemistry.

2.3. NO_x Conversion to HNO_3 in the High-Concentration Phase

[39] In addition to the chemical regimes described above, a fraction of the emitted nitrogen species is converted into HNO_3 within the plume. This conversion proceeds in two different ways.

[40] The first one takes place in daytime by the reaction of OH radical with NO_2. A large part of the OH radical originates from the photolysis of HONO (a species directly issued from combustion). The direct simulations of the species emitted during the aircraft fuel combustion show that the proportion of HONO represents approximately 5% of the emissions of the nitrogen species a few seconds after emission [*Kärcher et al.*, 1996; *Garnier et al.*, 1997; *Lewellen and Lewellen*, 2001]. We have evaluated the fraction β_1 of conversion of NO_x to HNO_3 with the box model. For a representative situation of flight conditions at cruise altitude this fraction is about 6%, reached after about 1 h for midday conditions. Since there are large uncertainties in the initial concentration of HONO [*Kärcher et al.*, 1996], that value of β_1 is also uncertain.

[41] The second path of conversion of the NO_x takes place mostly at nighttime, with the formation of NO_3, then N_2O_5. The latter is converted into HNO_3 by heterogeneous reactions on aerosols whose concentration is usually high inside aircraft plumes, and reaction on ice when contrails are formed. The fraction of NO_x conversion is thus directly related to the surface densities of the particles as well as their lifetime. Analytical and numerical calculations of aerosol surface densities have been done by *Kärcher* [1997]. For plume age of a few seconds the surface density is about $0.02\ m^{-1}$. As the plume expands the surface density decreases owing to dilution, scavenging by soot and eventually ice particle formation.

[42] For an aircraft wake representative of the modern jet aircraft, large-eddy simulations [see, e.g., *Paoli et al.*, 2008] show that the concentration of the ice particles is on the order of $10^9\ m^{-3}$ within the fresh contrails, with a mean radius of 1 μm. This gives a surface ice density of about $0.012\ m^{-1}$. For contrails that degenerate into "young cirrus" within an hour or so, observations [*Spinhirne et al.*, 1998] show that the concentration of ice particles is on the order of $3 \times 10^6\ m^{-3}$ with a particle size of 7 μm, corresponding to surface densities of $0.18 \times 10^{-2}\ m^{-1}$.

[43] Assuming that the probability of N_2O_5 heterogeneous reaction on ice is 0.03 and 0.1 on sulfate aerosols, as given by *Sander et al.* [2006], we evaluate from box model calculations that between 5% to 20% of the emitted NO_x is transformed into HNO_3 after approximately 12 h. This fraction of conversion, β_2, is thus very dependent on the formation and dispersion properties of the contrails. Indeed, if air is supersaturated, the concentration of ice particles is maintained for several hours, while in the case of dry air their evaporation is fast and the HNO_3 conversion limited. Using the MOZAIC aircraft data, [*Gierens et al.*, 2000] determined that at cruise altitude aircraft flies for 15% of the time into supersaturated air. For our calculations we have assumed that persistent contrails have a mean lifetime of 1 h and are formed with a probability of 0.15.

[44] To the authors' knowledge few data exist on persistent contrails transitioning into contrail-cirrus, while direct measurements of the concentration of HNO_3 are only available for relatively young contrails. The fractions of conversion β_1 and β_2 are thus very uncertain. *Kraabøl et al.* [2002] have determined the fraction of conversion using a Gaussian plume model. Depending on the turbulent conditions used, they found a percentage of conversion ranging from 20 to 53% at mid and high latitudes depending on the emission time, with the largest values at nighttime. Considering the simulations performed with our box model, and the results obtained by *Meijer* [2001], a fraction of nighttime conversion of 20% has been adopted. The β_1 and β_2 values used here are therefore in the medium range of previous evaluations and will be further discussed in section 3 along with the CTM results.

[45] With these assumptions the evolutions of the large-scale concentrations of NO_x and HNO_3 follow the equations

$$\frac{\partial r_{\overline{NO_x}}}{\partial t} + \left\langle F_{\overline{NO_x}} \right\rangle = \ldots + \frac{1}{\tau} \cdot \overline{r_f}(1 - \beta_1 \cdot \delta - \beta_2 \cdot (1 - \delta)) \alpha_{NO_x} \cdot EI \alpha_{NO_x} + \ldots \quad (32)$$

$$\frac{\partial r_{\overline{HNO_3}}}{\partial t} + \left\langle F_{\overline{HNO_3}} \right\rangle = \ldots + \frac{1}{\tau} \overline{r_f} \cdot (\beta_1 \delta + \beta_2 (1 - \delta)) \alpha_{NO_x} EI_{NO_x} + \ldots , \quad (33)$$

with $\beta_1 = 0.06$ and $\beta_2 = 0.2$.

2.4. Synthesis and Numerical Cases

[46] To account for the NO_x related chemical processes during plume dilution the proposed method implies that the

Table 1. Effective Rate Constant for O_3 Destruction at High NO_x Concentration[a]

NO_x (vmr)	K_{eff}, molecules^{-1} s^{-1} cm^3
1e-06	3.5 10^{-18}
5e-07	4.2 10^{-18}
1e-07	3.6 10^{-18}
1e-08	2.4 10^{-18}
2e-09	2.2 10^{-18}
1e-09	0.8 10^{-18}

[a]Computed for typical cruise conditions: 240 hPa and 230K; vmr is volume mixing ratio.

following system of equations is solved by the large-scale CTM:

$$\frac{\partial \overline{r_f}}{\partial t} + \langle F_f \rangle = I - \frac{1}{\tau}\overline{r_f}$$

$$\frac{\partial r_{\overline{NO_x}}}{\partial t} + \left\langle F_{\overline{NO_x}} \right\rangle = +\frac{1}{\tau}\overline{r_f}\,(1 - \beta_1\,\delta - \beta_2\,(1-\delta))\,\alpha_{NO_x}\,EI_{NO_x} + \ldots$$

$$\frac{\partial r_{\overline{HNO_3}}}{\partial t} + \left\langle F_{\overline{HO_3}} \right\rangle = +\frac{1}{\tau}\overline{r_f}\,(\beta_1\,\delta + \beta_2\,(1-\delta))\,\alpha_{NO_x}\,EI_{NO_x} + \ldots$$

$$\frac{\partial \overline{r_{O_3}}}{\partial t} + \langle F_{O_3} \rangle = -\left(\frac{1}{\tau}\left(\overline{NO_2}/\overline{NO_x} - E\right) + K_{eff}\,\overline{r_{O_3}}\,\rho\right)\overline{r_f}\,\alpha_{NO_x}\,EI_{NO_x}\,\delta + \ldots, \tag{34}$$

where I is given by the emission data set. EI_{NO_x} and the value of E depend on the combustion type, and must be consistent with I. The ratio $\overline{NO_2}/\overline{NO_x}$ is provided by the large-scale model in each computational box. The τ, β_1, β_2 and K_{eff} depend on the structure and the evolution of the plumes created after the injection.

[47] In a comprehensive approach, those quantities must be evaluated from explicit plume simulations. In the case of aircraft emissions, aircraft wake and contrail simulations have been performed in the near field [e.g., *Paoli et al.*, 2008] and in the mid and far field some tens of minutes after their injection [e.g., *Gierens*, 1996]. But there are very few simulations that have addressed the plume evolution and the transformation of contrails into young cirrus several hours after the injection. This is however the time horizon which is the most important to our parameterization, since O_x catalytic destroying cycles and NO_x conversion to HNO_3 are efficient on this time scale.

[48] Small-scale model simulations require very fine grids ($\Delta \sim 1-10$ m) to resolve the interactions between the exhaust jet and the wing-generated wake vortices, and the transition from the aircraft-induced turbulence to the atmospheric turbulence. To derive all parameters needed by the proposed parameterization, those models need to be integrated for several hours, and should include the microphysics for ice particle formation and a minimal chemical scheme such as O_3, NO_y, HO_x species with the related gas phase and heterogeneous reactions. Such comprehensive simulations are not yet available. However simplified approaches have been developed to estimate the dissipation and dilution processes of aircraft plumes. For example, *Schumann et al.* [1995] derived diffusion coefficients adapted to the diffusion of emissions during the dissipation of aircraft plume at the tropopause level. The magnitude of the horizontal coefficient was about 20 m^2 s^{-1}.

[49] Using this coefficient we have performed a simple 1D calculation where we compute the diffusion of a 250-m-wide plume and diagnose the value of τ from equation (3). Such an initial state is representative of the aircraft plume about 2 to 3 min after emission, at the end of the vortex regime [*Paugam*, 2008]. The results (see Appendix A) give a value of τ of about 16 h, corresponding to the dilution of the initial emissions by a factor 20. In addition to horizontal diffusion, vertical diffusion and wind shear have to be considered. Although the vertical diffusion is less efficient that the horizontal one, the vertical wind shear will tend to make the diffusion process more efficient [*Durbeck and Gerz*, 1996]. Given the range of variability for the wind shear and diffusion coefficient, the effective diffusion can vary by about 50% from a mean value of D_h = 15 m^2 s^{-1} [*Petry et al.*, 1998]. According to calculations performed with our 1D model this will give values of τ from 14 to 18 h.

[50] Since our determination of τ is related to the amplitude of the major perturbation in the NO_x/O_3 chemical system, it is worth to compare the above evaluations to outputs from chemical plume models. For instance, using a Gaussian plume model [*Meijer*, 2001] found that the nonlinear chemical effects last for about 15 h after the injection. Similarly, calculations from *Petry et al.* [1998] with a model of the same type, show that 12 h after NO_x injections the rates of ozone change during simulations that account for plume effects tend to the tendencies calculated assuming instantaneous dispersion. Therefore with different approaches we obtain a consistent range of numbers for τ, and a mean value of 15 h was adopted for most of our model simulations (section 3). However a much shorter value of 2 h was used in some 2D model simulations to test the model sensitivity to this parameter.

[51] The evaluation of K_{eff} requires the calculation of the integrals in equation (18) throughout the plume lifetime. As discussed above, such evaluations from small-scale models are not yet available. However with our chemical box model it is possible to explore the range of values that the K_{eff} coefficient can take as function of the NO_x loading. This has been done for typical conditions encountered by a jet aircraft at cruise altitude. The numerical values obtained from equation (29) are given in Table 1: K_{eff} varies from 1.0 to 4.2 $\times$ 10^{-18} molecules^{-1} s^{-1} cm^3, with a mean value close to 3.0 $\times$ 10^{-18} molecules^{-1} s^{-1} cm^3. The explored range for the values of the NO_x mixing ratio varies from 10 ppmv to 1 ppbv, so that it covers the values found during the dilution of the aircraft plumes from the vortex regime up to the diffusion regime [*Schumann et al.*, 1998].

[52] Another evaluation was performed using the 1D diffusion model described in Appendix A in which a minimum NO_x chemistry have been included (reactions (R2) to (R6) with O_3 photolysis). For a background O_3 content of 200 ppbv, an NO_x initial value of 20 ppbv and a mixing limit ratio limit r_l of 1 ppbv, a value of 2.5 $\times$ 10^{-18} molecules^{-1} s^{-1} cm^3 was obtained for K_{eff}. Thus, for the CTM simulations

reported in section 3 we have adopted the mean value of 3.0×10^{-18} molecules^{-1} s^{-1} cm^3.

3. Chemical Transport Model Simulations

[53] In this section the implementation of the plume parameterization detailed above in the 3D LMDz-INCA and 2D MOBIDIC chemical transport models is described. The various additional terms listed in the system of equation (34) are introduced and solved in the models, and the evaluation of the impact on the ozone change due to aircraft emissions is performed by comparing the results obtained with and without the plume parameterization. Results from the LMDz-INCA show the impact of the parameterization at global and regional scale, in particular in high-density air traffic zones within the flight corridors. Those results are complemented by those of the MOBIDIC model which is mainly used to measure the sensitivity of the parameterization to the prescribed parameters, namely the plume dilution time, the effective rate constant for ozone, and also the NO_x injection rate.

3.1. Model Descriptions

[54] The LMDz-INCA model simulates the transport of trace species and is coupled to the chemistry and aerosol model INCA (Interaction with Chemistry and Aerosols) developed initially by *Hauglustaine et al.* [2004] and extended by *Folberth et al.* [2006]. The model has 19 hybrid levels on the vertical from the ground to 3 hPa and a horizontal resolution of 2.5 degrees in latitude and 3.75 degrees in longitude. The large-scale advection of tracers is performed using the finite volume transport scheme of *van Leer* [1977] as described by *Hourdin and Armengaud* [1999]. Convective transport is simulated using Emanuel's mass flux scheme [*Emanuel*, 1991]. The INCA model is coupled online to the LMDz general circulation model nudged to the analyses of the European Centre for Medium-Range Weather Forecasting. INCA holds the surface and in situ emissions, calculates dry deposition and wet scavenging rates, and integrates in time the concentration of atmospheric species with a time step of 30 min. In addition to the CH_4-NO_x-CO-O_3 photochemistry representative of the tropospheric background, the NMHC version of INCA used here takes into account the photochemical oxidation pathways of nonmethane hydrocarbons (NMHC) and nonmethane volatile organic compounds (NMVOC) from natural and anthropogenic sources as well as their photochemical oxidation products. It includes 89 chemical species, 51 photochemical reactions and up to 280 chemical reactions, updated according to the compilation of *Sander et al.* [2006].

[55] The MOBIDIC model is a 2D model (altitude-latitude) covering the troposphere and the middle atmosphere up to the mesopause level [*Cariolle and Teyssèdre*, 2007; *Cariolle et al.*, 2008]. The chemistry scheme used in MOBIDIC includes the main gas-phase reactions driving the NO_x, HO_x, ClO_x, BrO_x catalytic cycles, with 30 transported long-lived species, and 30 short-lived species computed using steady state assumptions. The gas-phase chemical rates are also taken from *Sander et al.* [2006], with the additional inclusion of the HNO_3-forming channel from the HO_2+NO reaction [*Cariolle et al.*, 2008]. The model use a dynamical forcing from a transient scenario of the CNRM ARPEGE-Climat model. The MOBIDIC model adopts the residual meridional circulation formalism [*Dunkerton*, 1978] with the necessary heat and momentum fluxes derived from ARPEGE-Climat outputs for the period 1990–2000. Prather's advection scheme [*Prather*, 1986] is used for transport of the long-lived species, including the fuel tracer required for the plume parameterization.

3.2. Implementation of the Plume Parameterization

[56] To implement the plume parameterization the fuel aircraft NO_x emissions must be specified. To this purpose the database AERO2K provided by the Manchester University Center for Air Transport and the Environment [*Eyers et al.*, 2004] was used to get the fuel injection rate, i.e., source term of equation (1), in the prognostic equation related to the fuel tracer. The emissions inventories for the year 2002 have been used.

[57] The determination of the fraction of NO_x in the high-concentration plume form, equation (4), requires that NO_x emission be calculated from the fuel aircraft emissions using global mean emission indices. They were obtained using the total sums of the emissions, and not directly the grid-point values of the database. Therefore, these emission indices ensure a global injection of NO_x equivalent to what is given in the database, but with spatial distributions that can slightly deviate from those directly available in the database (with differences below 10% in most cases). In addition, two emission indices were computed corresponding to the civil and military aviation. A NO_x emission index of 13.2 g/kg was computed for the civil aviation, whereas military aviation gave a smaller value of 9.1 g/kg. As the military aviation represents a significant part of the emissions (10% of the total sum of the fuel aircraft emissions), two fuel tracers (and consequently, two prognostic equations) have been introduced in the LMDz-INCA model. For the sake of simplicity, the fuel aircraft emissions were supposed to be fully converted into NO aircraft emissions ($E = 0$ in equation (31)). The transport terms of the prognostic equations for the two tracers consider horizontal and vertical advections, diffusion in the boundary layer and convection. Dry deposition of the tracers is not introduced.

[58] The MOBIDIC model uses the same inventories data base from which zonally averaged emission rate values are derived, with no distinction between civil and military air traffic. Thus, a single fuel tracer is added to the prognostic equations with a single factor scaling $\underline{EI}_{NO_x}$, so only one continuity equation is solved directly for $r^p_{NO_x}$ (see equation (5)). Otherwise the global NO_x injection rates are identical in all the experiments made with the two models.

[59] Table 2 gives the list of experiments performed with the CTMs and the numerical values of the various parameters for implementation of the plume parameterization. Each model experiment consists in the difference between the outputs of two model simulations: a first one including the aircraft NO_x emissions and a second one corresponding to a reference simulation without any aircraft emissions. The experiment BC corresponds to the base case with aircraft emissions but without the plume parameterization. The experiment PL1 is performed with the parameterization but without the nitrification terms ($\beta_1 = \beta_2 = 0$) and PL2 includes all the terms of the parameterization. BC, PL1 and PL2 have been performed with both CTMs.

Table 2. Values of the Parameters for the Plume Parameterization

	Experiment						
	BC	PL1	PL2	PL3	PL4	BCx4	PL2x4
Model	2D and 3D	2D and 3D	2D and 3D	2D	2D	2D	2D
I_{NO_x} 2002	x1	x1	x1	x1	x1	x4	x4
τ	0	15 h	15 h	2 h	15 h	0	15 h
E		0	0	0	0		0
K_{eff}[a]		$3\ 10^{-18}$	$3\ 10^{-18}$	$3\ 10^{-18}$	0		$3\ 10^{-18}$
β_1		0	0.06	0.06	0.06		0.06
β_2		0	0.20	0.20	0.20		0.20

[a] K_{eff} units are molecules^{-1} s^{-1} cm^3.

[60] In order to explore the sensitivity of the results to some of the prescribed parameters of the parameterization, additional experiments have been conducted with the MOBIDIC model. Experiment PL3 is similar to PL2 except that the dilution time τ is reduced to 2 h. Experiment PL4 assumes that there is no ozone destruction within the plume ($K_{eff} = 0$). In addition, in order to investigate the behavior of the parameterization for larger NO_x emissions, a set of two experiments have been done with the NO_x injection rate multiplied by a factor of 4. Those experiments, BCx4 and PL2x4, use the same model configuration as BC and PL2, expect for the NO_x emissions.

[61] Each simulation of the of the LMDz-INCA model corresponds to an integration of 6 years over the period 2002–2007. To allow for model adjustments and spinup, the first year is discarded and monthly means outputs averaged over the last 5 years of the integration are used for the model analysis. The MOBIDIC simulations are integrated until a steady state is reached with stability of the monthly mean outputs. Ten years of integration are typically required, and the model analysis is conducted using the outputs from the last year.

3.3. Simulations of Aircraft NO_x Emissions and Dispersion

[62] Two simulations were first performed with the LMDz-INCA model to evaluate the influence of τ on the tracer fuel distribution. Figure 2 shows the zonally averaged (top) fuel concentration for the second year of the simulation and its geographical distribution at 240 hPa (bottom) for July and for two plume lifetimes, 2 h (left) and 15 h (right).

[63] The fuel aircraft emissions are mainly produced over Northern Hemisphere continents around 40°N. They induce local maxima for the fuel concentration at cruise altitude but also at the surface. This suggests that τ and K_{eff}, whose values have been evaluated for the cruise altitude, should eventually depend on altitude. Owing to those limitations in the implementation of the parameterization, the analysis is focussed on the middle and upper troposphere, above the 600 hPa level. At cruise altitudes the fuel concentration is mainly confined along the aircraft routes, and reaches maximum values over the NAFC, North America, Europe and the Far East. A significant increase in fuel concentration can be noted when the plume lifetime is enhanced from 2 h to 15 h. This increase corresponds to the factor of about 15/2 in the peak concentration regions, which means that the tracer distribution follows a regime of quasi-linearity as a function of plume lifetime. Consequently, as the second term in the ozone continuity equation (30) is proportional to $\overline{r_f}$, the associated ozone tendency is expected to be proportional to τ in regions of dense traffic.

3.4. Impact of Aircraft NO_x Emissions on the Ozone Distribution

[64] Figures 3 and 4 show the zonally averaged NO_x and O_3 changes (Figures 3 and 4, top) due to aircraft emissions for July and January of the BC experiment. The same changes at the 240 hPa level (Figures 3 and 4, bottom), near cruise altitude, are also shown.

[65] As expected, the aircraft-induced NO_x increase is mainly localized in the Northern Hemisphere at and above the tropopause. Outputs from the LMDz-INCA model shows maximum values around 25 pptv in July for zonal means. At cruise altitudes, this enhancement is maximum along the NAFC, over North America and over Europe where NO_x change reaches up to 60–70 pptv. This aircraft-induced NO_x increase leads to O_3 increase mainly in the Northern Hemisphere and in the upper troposphere. The maximum O_3 enhancement reaches values around 2.5 ppbv for zonal means, corresponding to a relative change between 2.5 and 3%. At 240 hPa, the O_3 increase is confined along the heavy corridors (NAFC), and over North America and Europe with a maximum of 3.2 ppbv. The MOBIDIC model shows a consistent picture (Figure 5), with a maximum NO_x increase of about 22 pptv, and an associated O_3 in the range 2 to 4 ppbv, about 3–4.5% in relative terms.

[66] In January (Figure 4) the LMDz-INCA model exhibits the same characteristics than in July with less concentrated ozone production within the NAFC. This results from a decrease in the ozone production by the NO+HO_2 reaction in winter compared to summer time, and to a faster circulation in the NH winter that transport and mix the ozone produced more vigorously. The MOBIDIC model gives an ozone increase larger than the LMDz-INCA model at cruise altitude, but shows less production below the 500 hPa level. Overall the two models gives relative O_3 increases in the range 2 to 3%.

[67] The amplitude and distribution of the ozone response to the NO_x aircraft emissions is consistent for the two models with previous estimates. For example, *Meijer* [2001], using the TM3 CTM to evaluate the impact of the 1997 air traffic, found an increase of the NO_x content of about 90 pptv/50 pptv in the NAFC for the months of January/July, leading to an ozone increase of about 2 to 3 ppbv at mid and high latitudes in the NH. Those figures agree also with the previous evaluations by *Brasseur et al.* [1996, 1998]. *Brasseur et al.* [1996] reports an O_3 maximum increase of 1.3% in January and 4% in July near the NAFC for the 1990

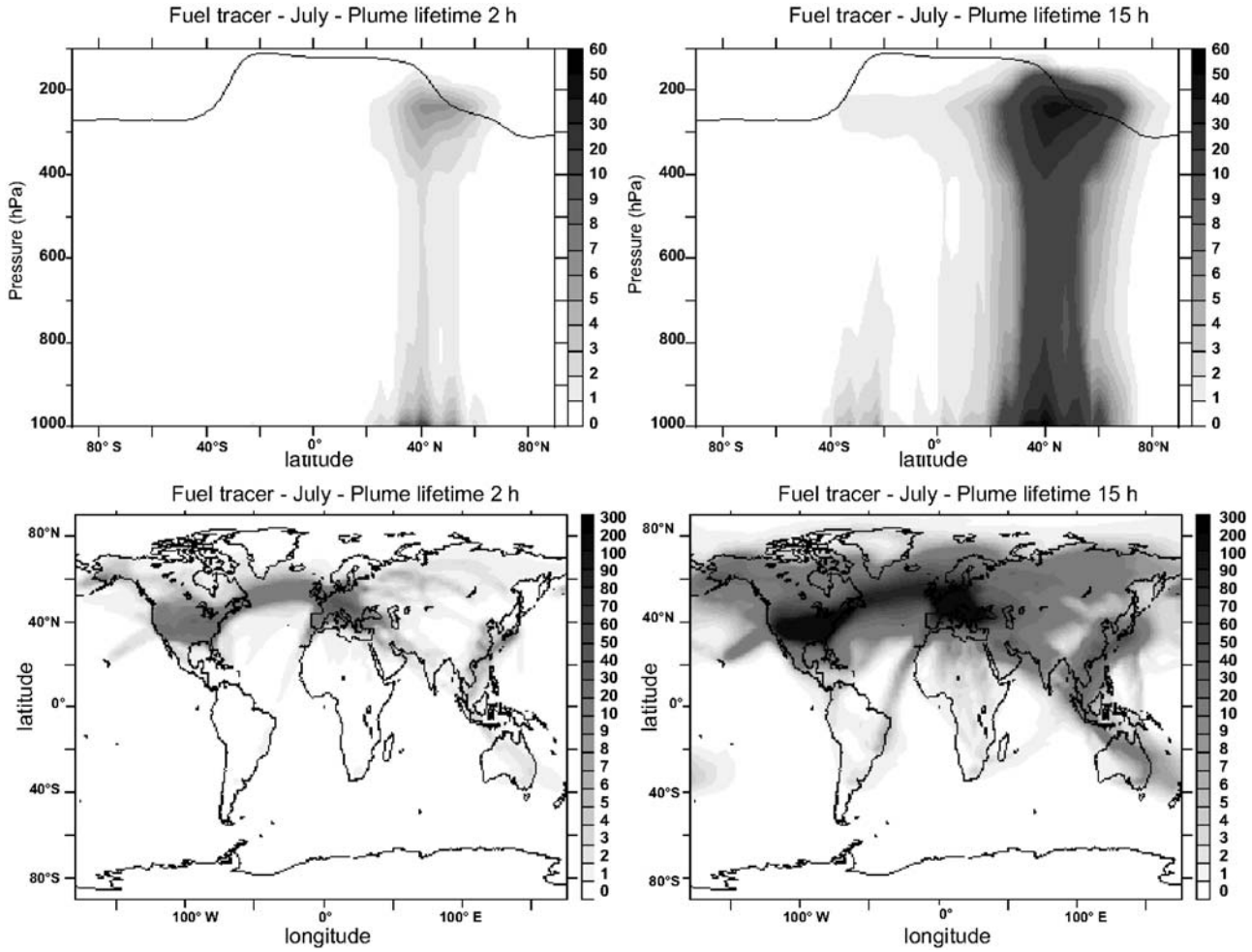

Figure 2. (top) Zonally averaged fuel concentration and (bottom) its geographical distribution at 240 hPa for July and for two plume lifetimes, (left) 2 h and (right) 15 h. Results from the second year of the LMDz-INCA model simulation. Units are in 10^{-17} Kg cm^{-3}.

fleet. Similarly, *Brasseur et al.* [1998] give the results of the simulations by 4 CTMs of the ozone increase due to the 1990 aircraft fleet. Those models calculate maximum ozone perturbations within the range 4–9 ppbv in summer and 1.5–5 ppbv in winter.

[68] Figures 6 shows the zonally averaged NO_x and O_3 changes at the 240 hPa level computed with the LMDz-INCA model for experiment PL1 compared to experiment BC. PL1 includes the plume parameterization without nitrification (see Table 2).

[69] As expected, at cruise altitudes near the tropopause, the use of the parameterization of plume chemistry delays the release of the NO_x aircraft emissions at large scale and leads to a decrease of the zonal mean NO_x change up to 2–3 pptv (between 5 and 10%) compared to experiment BC. This effect is larger within the flight corridors, with up to 20 pptv change, and corresponds to a diminution of 30% of the NO_x increase due to the aircraft emissions.

[70] Since the aircraft emissions inside plume are not instantaneously converted into large-scale NO_x, they are affected by large-scale transport. Thus, they can be advected in remote regions, possibly far from those where they have been produced, and then released to feed the large-scale NO_x content. In other words with the parameterization the delay of several hours in the release of the emissions in form of large-scale NO_x, allows the transport of the aircraft emissions in plume form, and consequently we obtain both a diminution of the large-scale NO_x increase near the corridor region and its growth in regions free of direct aircraft injection.

[71] Consequently, a decrease in the O_3 production in regions of high density of aircraft traffic and possible increase in more remote regions are expected. This is confirmed by the LMDz-INCA model results, with an O_3 zonal mean production decreasing by 20 to 90 pptv at cruise altitudes owing to the smaller NO_x and the additional loss rate associated to the K_{eff}. The geographical distributions of the changes in concentrations at the 240 hPa level show that the plume effects decrease the O_3 production along the heavy aircraft corridors up to 140 pptv over Europe, and up to 300 pptv over North America. In terms of relative effect, the O_3 production is reduced by 2 to 9% within the NAFC, with the largest impacts in July over the western United States and central Europe. Over Asia, the impact is lower in absolute terms, about 60 pptv, but on the same order for the relative diminution of the O_3 increase, about 8 to 10%.

[72] In addition, there is a region, south of the NAFC corridor, where plume transport induces an enhancement of

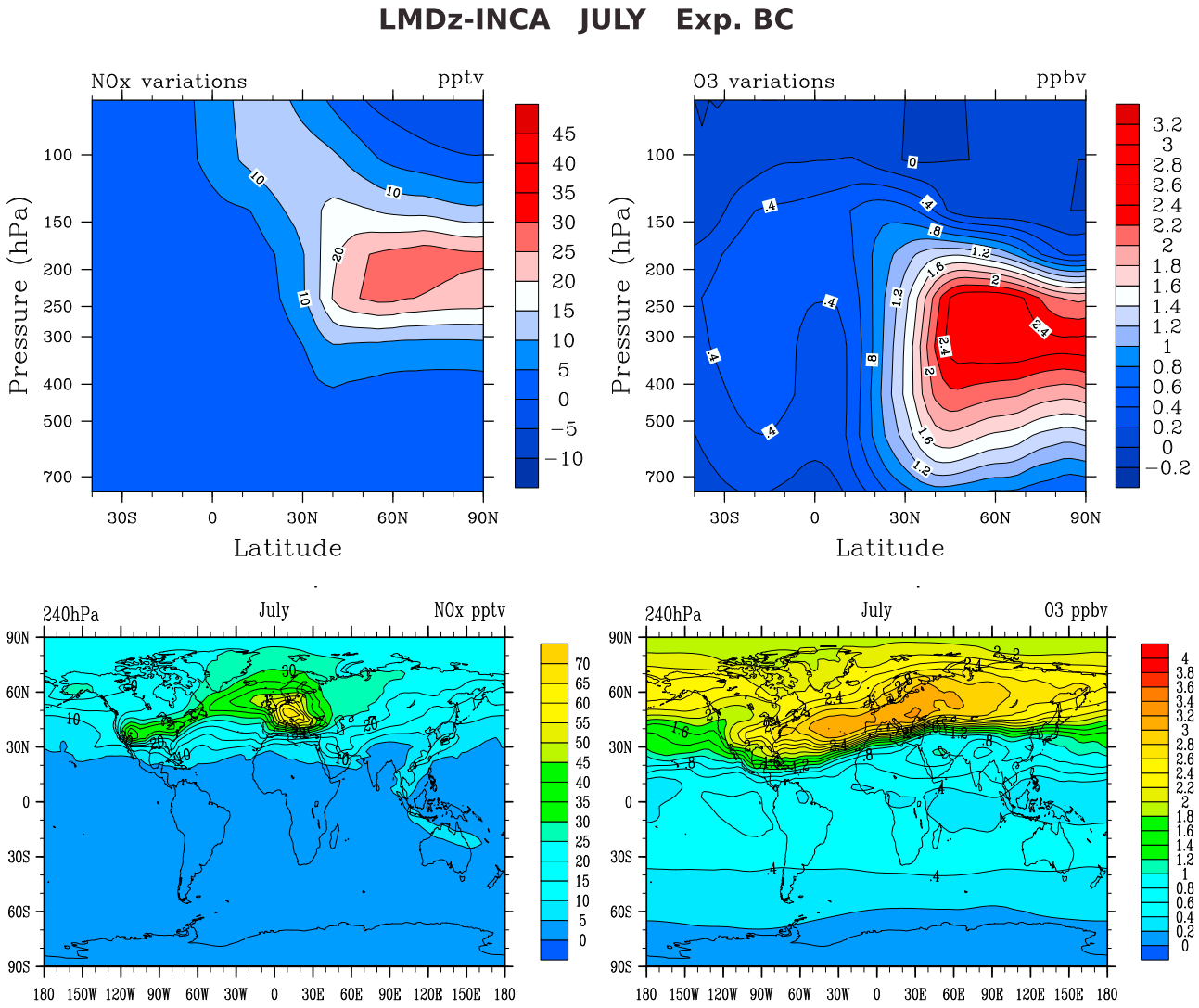

Figure 3. (top) Zonally averaged (left) NO_x and (right) O_3 changes due to aircraft emissions and (bottom) their geographical distributions at 240 hPa for July. Experiment BC with the LMDz-INCA model.

the NO_x content and increases the O_3 production, up to 60 pptv for O_3. This region tends to extend over central America up to Australia via the south of the African continent. This illustrates the effect of the plume transport that can release the emitted NO_x far from the routes of heavy aircraft traffic. Similarly, in July at high latitude, there is an increase in the O_3 production in the middle troposphere below the cruise altitude by about 40 ppb, in the 3 to 5% range. This is also due to the transport of the plumes by the mean meridional equator to pole circulation. Examination of the model outputs for each individual year shows a high stability of the results in the corridor areas. This is due to the use of fixed routes and monthly mean NO_x injection rates. Outside those regions, there is more variability associated to the characteristics of the transport for a given year, but the general patterns and amplitudes for the ozone variations remain from one year to another.

[73] The MOBIDIC model (Figure 7, top) shows similar responses to the LMDz-INCA model for the zonal mean diagnostics. The ozone increase due to NO_x injections is reduced by 7 to 11% at the tropopause level in the NH, with similar reductions extending to the entire middle troposphere in January at midlatitudes.

[74] In summary, the PL1 experiments shows that the impact of NO_x titration and O_3 destruction inside the plumes introduced via the K_{eff} coefficient are mostly significant in the NAFC, whereas the transport of the plumes by the large-scale circulation impact the O_3 production over the entire Northern Hemisphere and in some specific regions in the Southern Hemisphere. The magnitude of the global effect peaks to 5 to 12% in the regions of the largest O_3 changes.

[75] As discussed in section 2, the conversion of NO_x into HNO_3 is not negligible in the aircraft plumes due to the enhanced concentrations of aerosols and ice particles. To evaluate the impact of this conversion the PL2 experiment has been performed with the plume parameterization including all the terms of the system of equation (34), with the values of the conversion fractions β_1 and β_2 given in Table 2. Otherwise the experiment has been conducted in similar conditions to the PL1 experiment.

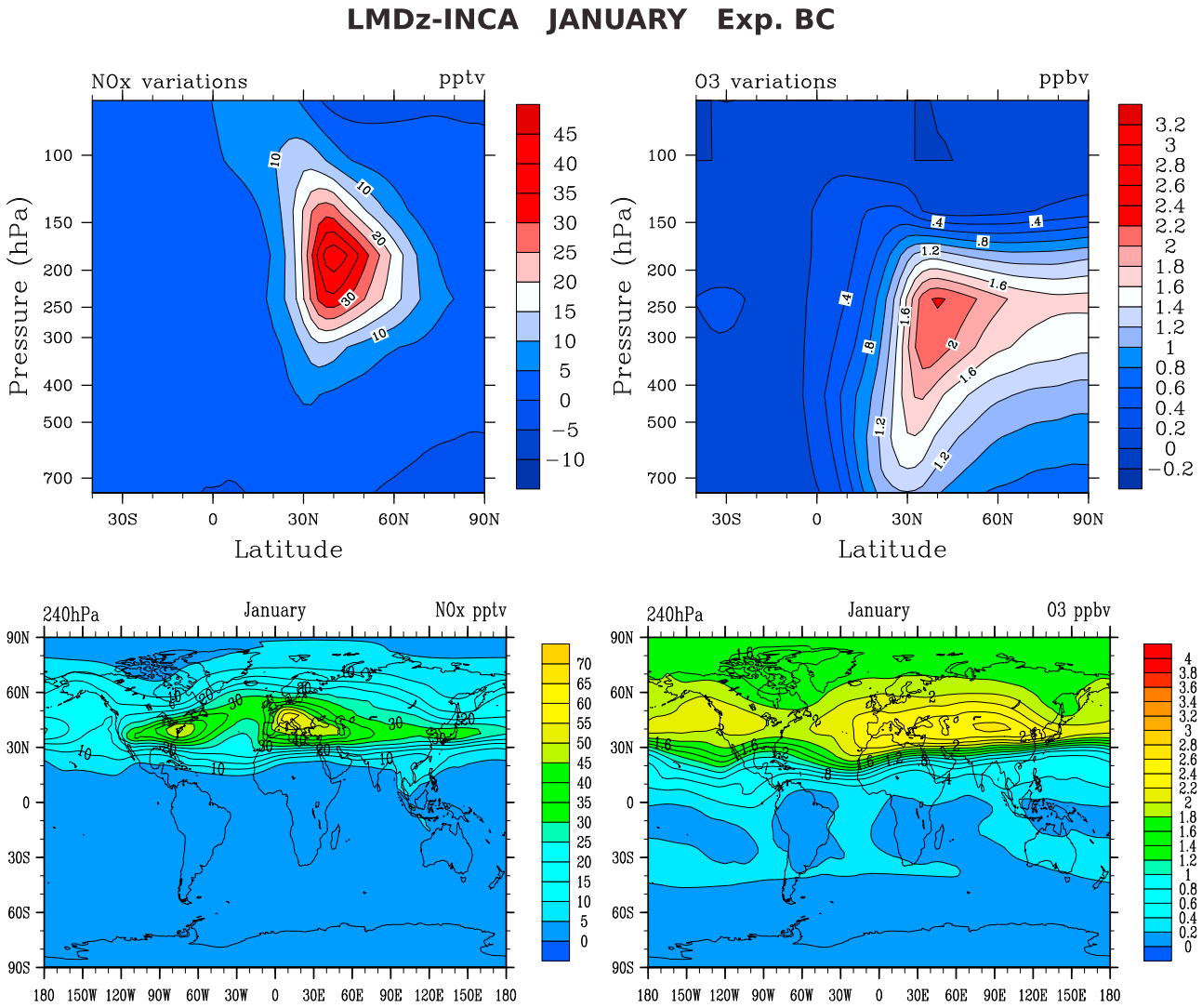

Figure 4. (top) Zonally averaged (left) NO_x and (right) O_3 changes due to aircraft emissions and (bottom) their geographical distributions at 240 hPa for January. Experiment BC with the LMDz-INCA model.

[76] Figure 8 shows the impact of the full parameterization on NO_x and O_3 changes at cruise level from the LMDz-INCA model simulations. As expected the account for nitrification increases the impact of the plume parameterization. This is to be expected since in addition to the mitigation of the local O_3 increase, and to the transport induced NO_x emissions in plume form, the transformation of a fraction of NO_x into HNO_3 increases the storage of the emitted NO_x into a reservoir species that has a rather long lifetime (up to 1 month in the upper troposphere in winter time at midlatitudes). As a result the PL2 experiment shows similar regional patterns as PL1 but with an enhanced response.

[77] At cruise altitude in the NAFC region the plume effects lead to a decrease of the large-scale NO_x up to 24 pptv, and a reduction of the O_3 increase up to 460 pptv. In relative numbers the O_3 production due to the NO_x emissions is decreased by about 5% in July and up to 12% in January for the whole NH (Figure 9). The reduction of the O_3 production reaches 25% in the NAFC and Asian regions.

[78] The PL2 experiment shows larger impact (almost a factor 3) of the plume parameterization than PL1 in the winter season, whereas the two experiments show less differences in summer. This is a direct consequence of the HNO_3 formation that is enhanced in winter season owing to longer night periods, associated to a longer lifetime due to the decreasing efficiency of its photodissociation in wintertime. Zonal mean diagnostics (Figure 9, left) show that the large-scale NO_x increase is reduced by up to 8% in July and 15% in January in the upper troposphere with the PL2 experiment compared to the BC experiment.

[79] The MOBIDIC model gives results for the PL2 experiment in agreement with the LMDz-INCA simulations. The zonal mean ozone increase in the NH (Figure 7, middle) is reduced by about 12% in July and 18% in January compared to the BC one, so with a sensitivity to the plume parameterization slightly larger than the LMDz-INCA model.

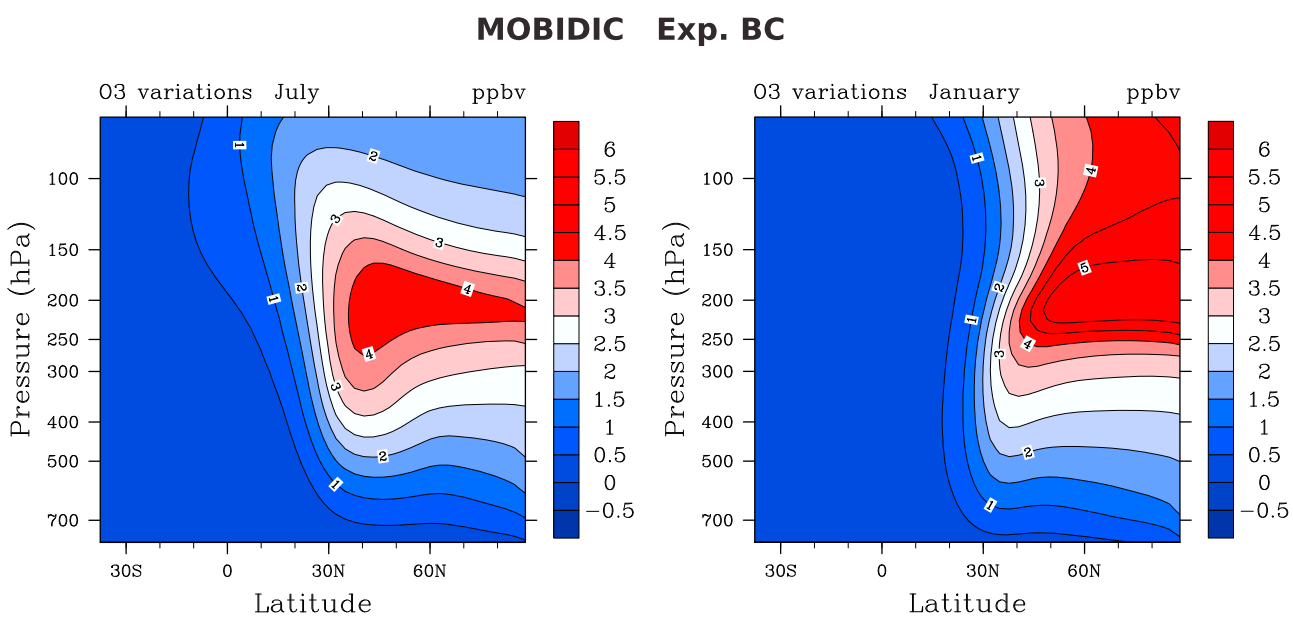

Figure 5. Zonally averaged O_3 changes due to aircraft emissions for (left) July and (right) January. Experiment BC with the MOBIDIC model.

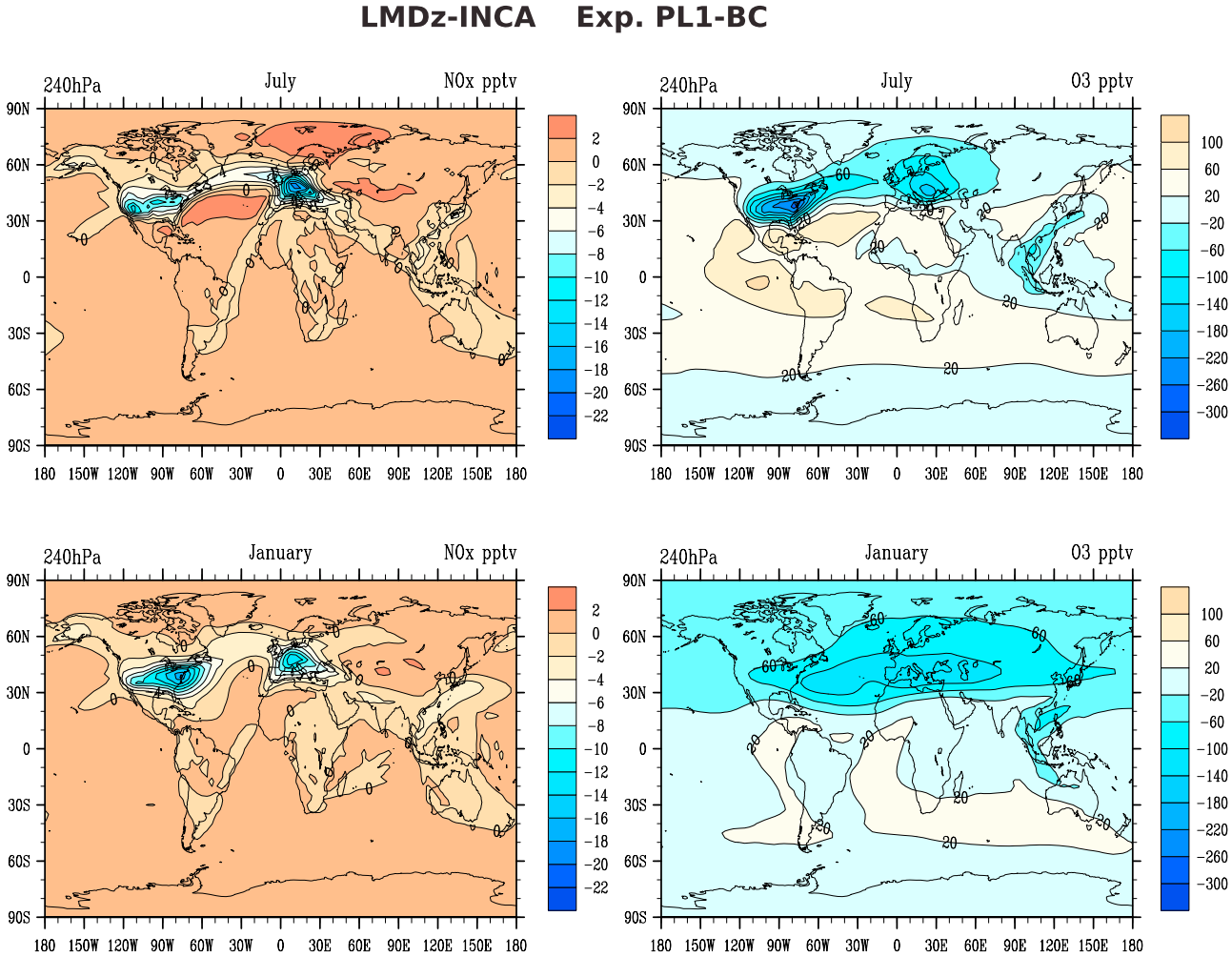

Figure 6. Distribution of the (left) NO_x and (right) O_3 variations at 240 hPa due to plume effects for experiment PL1 relative to the experiment BC. Results from the LMDz-INCA model for (top) July and (bottom) January.

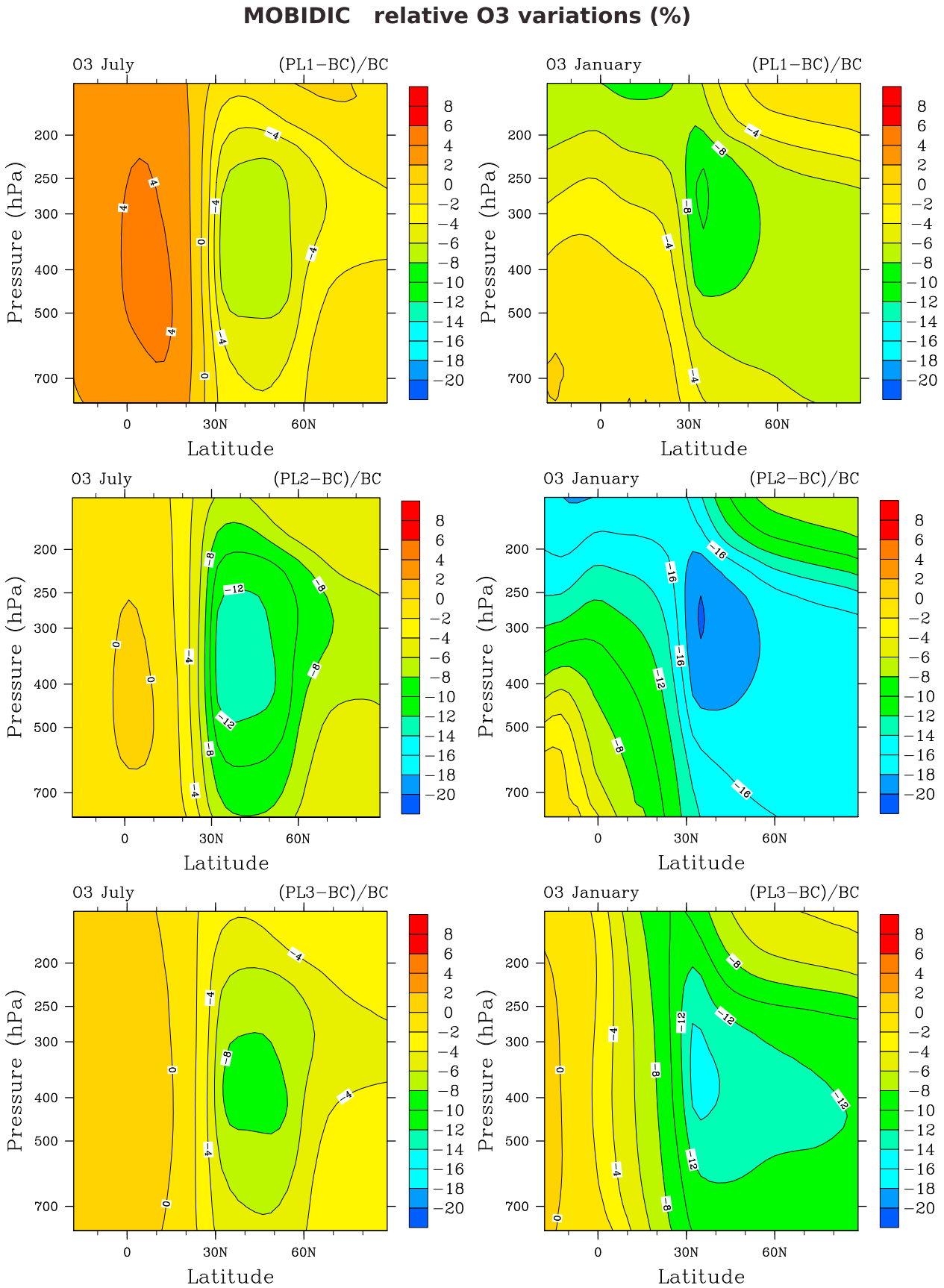

Figure 7. Zonally averaged relative O_3 changes due to plume effects for (left) July and (right) January. Results from the MOBIDIC model. Experiments (top) PL1, (middle) PL2, and (bottom) PL3 relative to experiment BC.

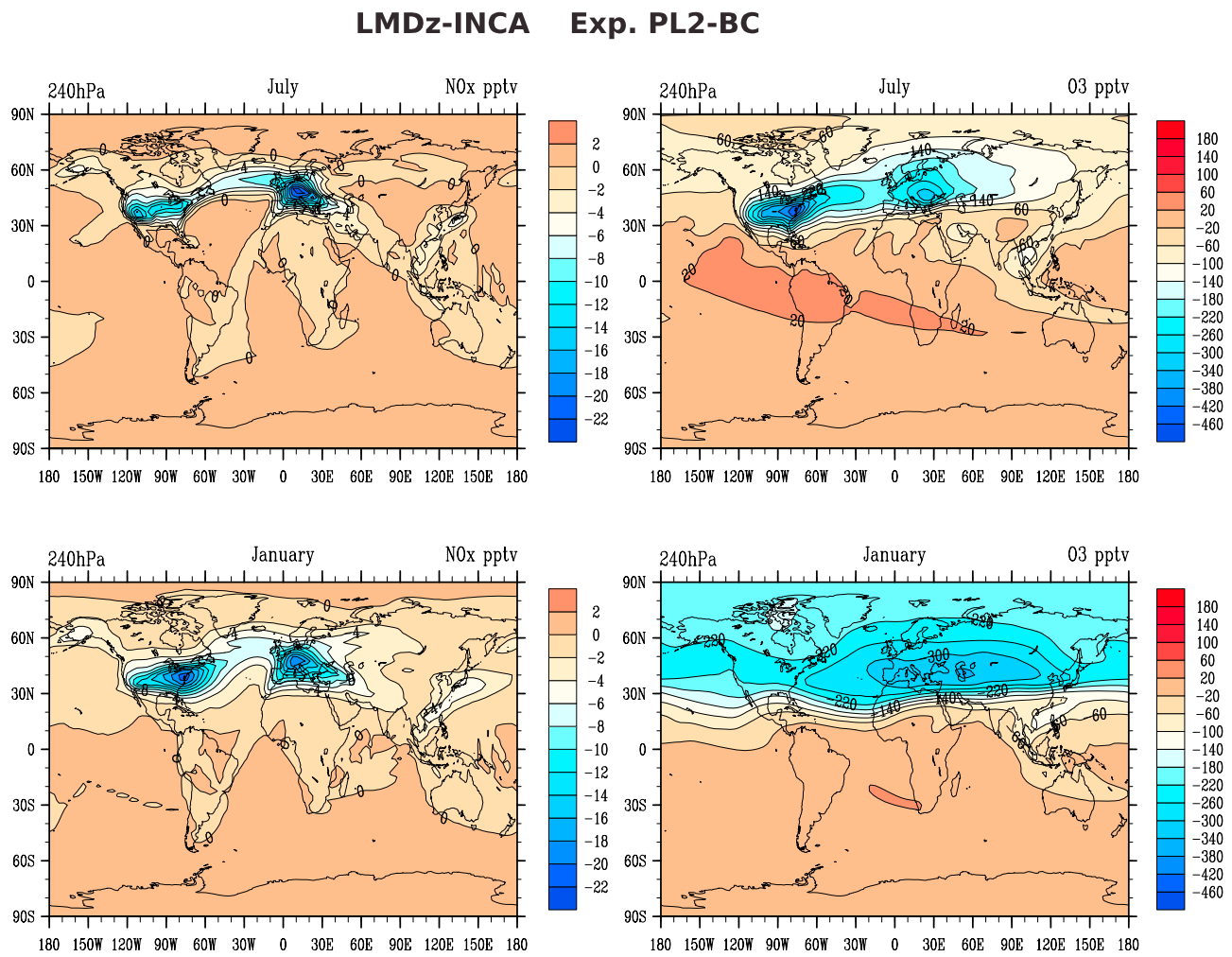

Figure 8. Distribution of the (left) NO_x and (right) O_3 variations at 240 hPa due to plume effects for experiment PL2 relative to the experiment BC. Results from the LMDz-INCA model for (top) July and (bottom) January.

In addition, the MOBIDIC model shows a behavior in agreement with the LMDz-INCA model when nitrification is taken into account. The comparison between experiments PL1 and PL2 (Figure 7, top and middle) shows that the parameterization of the nitrification within the plumes further decreases the O_3 formation by 6% in July and up to 10% in January. Those figures compare well with the outputs from the LMDz-INCA model.

[80] The two models use very close chemical schemes, but have very different representations of the transport by the large-scale dynamics and the unresolved processes, like convection and diffusion. So they show differences in the global distributions of the key trace species, and we do not expect that the two models would exhibit exactly the same sensitivity to the plume parameterization. Rather, the two models have comparable responses, showing the robustness and the relative independence of the parameterization to the details of the CTM in which it is implemented.

[81] The results of our modeling experiments are also consistent with the results of models that use effective emissions or correction factor formulations. *Meijer* [2001] reports reductions of the O_3 increase of about 5% in January and up to 10% in July in the NAFC when emission conversion factors are implemented in his CTM calculations. Similarly, *Kraabøl et al.* [2002] performed simulations with a global CTM including conversion factors. They found reductions of the NO_x perturbation by 15 pptv and O_3 perturbation by 500 pptv in the NAFC, and a decrease in the ozone production in the range 15–18% at northern middle and high latitudes. Those figures are in good agreement with the present evaluations.

[82] Apart from the representation of nitrification, our parameterization is based on few key parameters, namely the dilution time τ and the effective rate constant K_{eff} for the ozone destruction within the plume. Using the MOBIDIC model we have performed sensitivity experiments to those parameters. Experiment PL3 was performed with a shorter time, τ = 2 h instead of 15 h, and experiment PL4 with the suppression of the ozone destruction within the plume (K_{eff} = 0). Table 2 details the parameters values set for the different experiments and Table 3 summarizes the results for the ozone sensitivity.

[83] As expected the reduction of the dilution time lessen the impact of the plume parameterization, by a factor of about

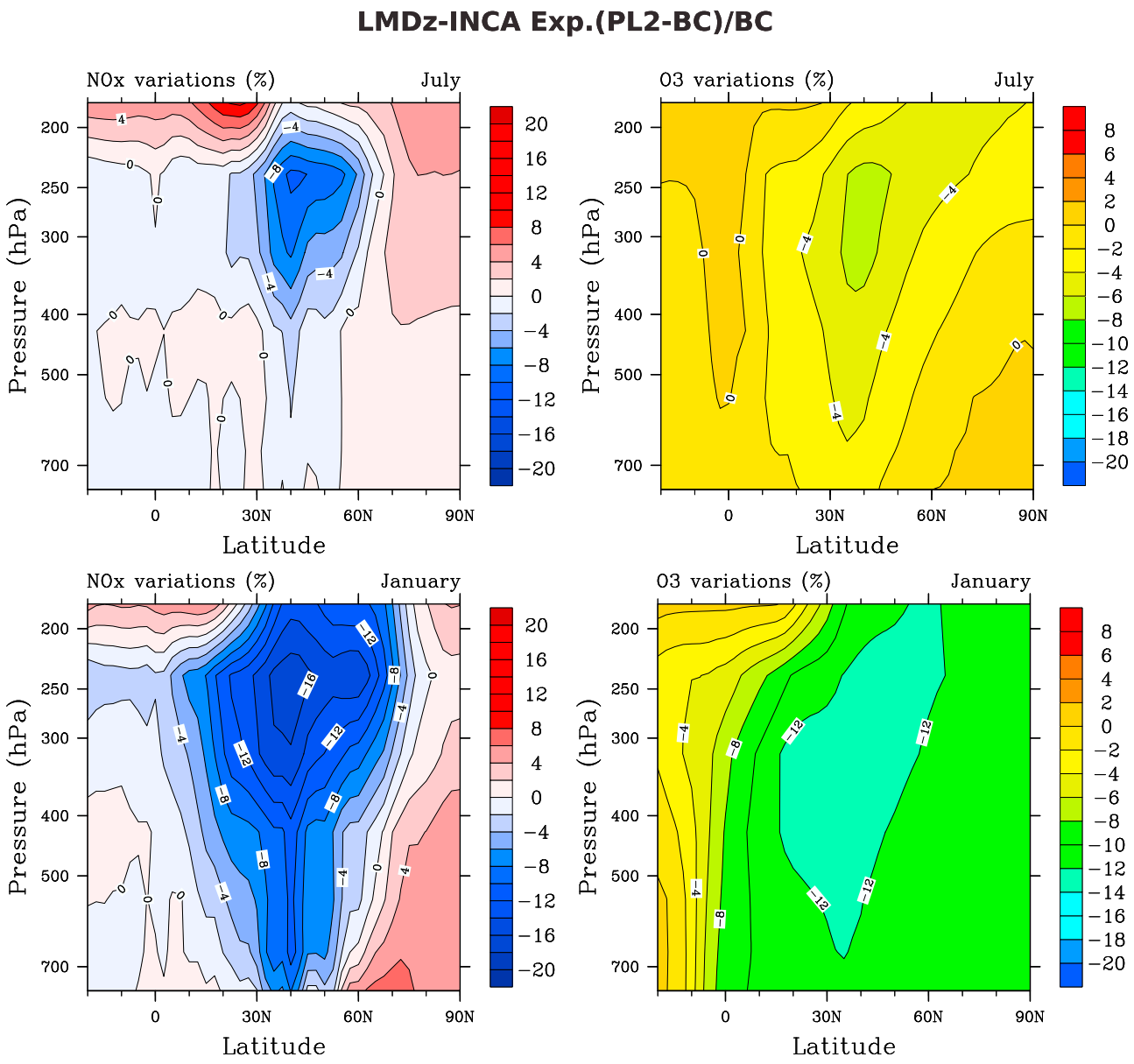

Figure 9. Zonally averaged relative (left) NO_x and (right) O_3 changes due to plume effects for (top) July and (bottom) January. Results from the LMDz-INCA model, experiment PL2 relative to experiment BC.

1.5. A shorter dilution time gives less NO_x stored in the high-concentration phase, so a larger large-scale NO_x with subsequent O_3 production via reaction (R1), and induces less O_3 destruction via the last term of equation (30). So the result is a reduction of the efficiency of the plume parameterization, with the PL3 experiment giving model sensitivities to the plume effects close to those of the PL1 experiment.

[84] Similarly, the PL4 experiment shows a reduction by a factor 1.3 of the O_3 change induced by the parameterization compared to the PL2 experiment. The parameterization appears to be slightly more sensitive to the prescribed dilution time than the value of the O_3 destruction rate within the plume.

Table 3. Maximum Reduction in Zonal Mean Ozone Formation due to the Introduction of the Parameterization of Plume Chemistry Into the MOBIDIC Model[a]

	Experiment				
	(PL1-BC)/(BC)	(PL2-BC)/BC	(PL3-BC)/BC	(PL4-BC)/BC	(PL2x4-BCx4)/(BCx4)
January	−11%	−22%	−15%	−17%	−19%
July	−7%	−13%	−9%	−11%	−11%

[a]See text for definition of experiments BC, PL1, PL2, PL3, PL4, BCx4, and PL2x4.

[85] All the previously described model simulations have used the emission inventories for the year 2002. In the future the air traffic is expected to grow significantly, and we have therefore evaluated how the plume parameterization would respond to an increase of the aircraft NO_x emissions. Using the MOBIDIC model we have performed the BCx4 and PL2x4 experiments in which the fuel tracer injection rate, I in equation (1), has been multiplied by a factor 4 without and with, respectively, activation of the parameterization (see Table 2). Interestingly the O_3 sensitivities to the parameterization are very close for PL2x4 and PL2 (Table 3). This means that in relatives terms the mitigation effects on O_3 production of the plume chemistry will work with the same intensity regardless of the details of the adopted injection scenario. At least as far as the air traffic follows the same major routes.

4. Discussion

[86] The simulations reported here show that the proposed parameterization of plume effects applied to aircraft NO_x emissions gives results that are consistent with previous works based on modification of the emission indices, or the calculation of conversion factors to be applied in the continuity equations of trace species.

[87] In the present approach it was chosen to implement our parameterization using a restricted number of predetermined parameters, the K_{eff}, τ and β coefficients, that were determined on the basis of simple model simulations and representations of the atmospheric processes.

[88] The method itself could be first improved by using more than one phase to describe the evolution of the fraction of the emissions at high concentration. Instead of fixing only one value for the threshold mixing ratio r_l that determine the boundary of the plume, several values corresponding to various degrees of dilution could be introduced. For example if two values, $r_{l1} > r_{l2}$, are used two tracers and values of τ will be introduced, extending the system to two fuel tracers,

$$\begin{aligned} \frac{\partial r_{f1}}{\partial t} + \langle F_{f1} \rangle &= I - \frac{1}{\tau_1} r_{f1} \\ \frac{\partial r_{f2}}{\partial t} + \langle F_{f2} \rangle &= \frac{1}{\tau_1} r_{f1} - \frac{1}{\tau_2} r_{f2}. \end{aligned} \tag{35}$$

The values of τ_i would be obtained using equation (3) in decomposing the mass fraction $M(t)$ in two phases corresponding to the two dilution fractions. The result would be a better fit of the representation of the dilution process. For the example given in Appendix A the introduction of two phases with dilution ratios from 1 to $r_{l1}/r_p(t_0) = 0.1$, and from 0.1 to $r_{l2}/r_p(t_0) = 0.05$, improves the approximation of the mass evolution $M(t)$ from 20% to about 10%.

[89] In addition, different values for K_{eff} could be associated to each fraction, so the determination of the ozone tendencies due to the plume effects, $R = -\Sigma_i[K^i_{\text{eff}}\ \overline{r_{O_3}} \rho r_{fi} \alpha_{\text{NO}_x} EI_{\text{NO}_x}]$, would be also more accurate. Similarly, the values of β could be determined for each phase, resulting in a better evaluation of the rates of HNO_3 formation within the plume. Thus, the extension of the method with the introduction of multiple phases to describe the plume dilution requires to add one fuel tracer for each regime. This appears affordable for the already complex large-scale CTMs.

[90] Further developments of our method would be required to improve the consistency between the different parameters and the physical parameterizations and the chemical system implemented within the CTMs.

[91] In particular, the dilution time scale τ should eventually depend on the level of turbulence within each grid cell of the CTM. It could be function of the effectiveness of the dilution and be linked to the stability, average wind shear, and the turbulent kinetic energy or the turbulent diffusion coefficients, depending on the formulations employed by the large-scale model. For example a Gaussian plume model [*Konopka*, 1995] could be used to compute the time evolution of $M(t)$ in equation (2) with the diffusion coefficients related to the Brünt-Väisällä frequency and the vertical shear from the large-scale model, as proposed by *Durbeck and Gerz* [1996].

[92] Similarly, the β coefficients could be related to the subgrid parameterized physic of the large-scale model and the humidity content of the model atmosphere. In particular some models now include microphysical parameterizations that account for supersaturation, like the ECMWF model [*Tompkins et al.*, 2007]. In supersaturated air the ice particles formed within the contrails would be maintained when they are transformed into contrail-cirrus, and the NO_x conversion to HNO_3 would be enhanced. However the heterogeneous processes due to the aerosols could be suppressed when ice particles are formed within the plume, so the net result can be only predicted using detailed microphysics and heterogeneous chemistry plume model. *Meilinger et al.* [2005] have used such a model to calculate NO_y Emission Indices and their dependance on local atmospheric composition, their model could equally be use to derive β parameters consistent with the plume lifetime. In the same way, the K_{eff} coefficient should depend on pressure and temperature computed by the CTM.

[93] All those refinements in the implementation of the plume parameterization would be of course most valuable for three-dimensional models with resolutions good enough to represent the atmospheric variability at the synoptic scale. Thus, there are prospects to improve the parameterization provided that small-scale plume simulations and/or atmospheric observations can give the necessary input data to link the parameters to the large-scale state of the atmosphere. The models that are able to represent the dilution phase of aircraft wakes and contrails are now developed [*Gierens*, 1996; *Durbeck and Gerz*, 1996; *Lewellen and Lewellen*, 2001; *Paoli et al.*, 2008; *Paugam*, 2008] and they can give some of the necessary data.

[94] The basic principles of the parameterization can be applied to any NO_x emission by a point source provided that the plumes formed are enough isolated until dilution in the background atmosphere. This is mainly the case for aircraft plumes, but also for instance for ship plumes whose life cycle follows stages of formation and dispersion in the marine boundary layer. Recently, *Chosson et al.* [2008] have

conducted ship plume simulations corresponding to various state of the boundary layer in the marine atmosphere and have calculated dilution time function of convective activity. Their calculations could be used to prescribe the parameters needed by our parameterization. NO_x and O_3 perturbation have been reported owing to ship activity, [i.e., *Schlager et al.*, 2006], and K_{eff} for ozone could therefore be determined.

5. Conclusions

[95] A new formulation that accounts for the transformation of emissions and their chemical reactions has been proposed to parameterize the plume NO_x chemistry into large-scale models. The main features of this approach are that it is mass conservative by construction, and that it accounts for large-scale transport and the nonlinear chemical reactions within the plumes that impact the large-scale O_3 concentrations. It can be easily implemented in large-scale models, with the additional computational cost associated to the introduction of one additional tracer.

[96] The derived parameterization has been introduced in the LMDz-INCA and MOBIDIC models to study the impact of present-day aircraft activity on atmospheric ozone. It is found that the plume-induced effects lead to significant mitigation of the global ozone production by the aircraft NO_x emissions. The major effect is to decrease the ozone production within the NAFC and over the Asian region dense of aircraft traffic by about 15 to 25%. In those regions the reduction in the O_3 production is dominated by the enhanced activity of the ozone destroying cycles that prevails at high NO_x concentration. Otherwise in adjacent regions and at high latitudes in the NH, the partial transformation of the emitted NO_x into HNO_3 plays an important role. Since HNO_3 has a longer lifetime in winter, the larger impacts of the parameterization are found for this season with a reduction in the O_3 increase of 10% for the whole NH. At lower latitudes and in the SH, in regions free of direct emissions, the ozone production can be increased owing to the release of NO_x in plume form after transport by the large-scale circulation. Overall, the results obtain with both models are consistent with previous studies that have used effective emission indices or conversion factors to the aircraft emissions.

[97] In the future, improvements of the parameterization are expected on the basis of better evaluations of the required parameters by small-scale model simulations and atmospheric observations. In particular, the plume lifetime and the effective reaction rates should be made dependent on local turbulent properties, on temperature and humidity. In addition, the developed framework could be also extended to treat different phases during the plume dispersion, at the expense of additional tracers, characteristics times and effective O_3 reaction rates for each phase.

[98] The parameterization might be also adapted to treat other types of local NO_x emissions, like for instance the ship plumes evolution in boundary layers. For nonisolated emitting sources, like power plants and cars in dense urban cities it is not easy to evaluate the feasibility of our approach since it is difficult to isolate specifically the plumes and to determine their lifetime. However the possibly of introducing effective reaction rates working on fractions of the emitted species could still be adopted, but would be more complex to constraint by small-scale modeling and measurements.

Appendix A

[99] Using a simple example we illustrate here the necessary steps to evaluate the values of τ and K_{eff} from a small-scale plume simulation. The dilution process is simply represented by the horizon diffusion of a plume 250 m wide with a diffusion coefficient D = 20 m^2 s^{-1}. These values are typical of initial aircraft plume size a few minutes after emissions and of diffusion properties at the tropopause level. Vertical diffusion and shear advection are neglected. An initial tracer with uniform mixing ratio $r_p(t_0)$ = 20 ppbv is introduced at the beginning of the simulation and plume boundary is defined by the mixing ratio r_l = 1 ppbv.

[100] Figure A1 (left) shows the time evolution of the normalized tracer distribution $r_p/r_p(t_0)$. The isoline $r_l/r_p(t_0)$ = 0.05 marks the evolution the plume boundary. The size of the plume, l_p, increases from 250 m up to a maximum of 2250 m after 10 h, and then decreases afterward to disappear completely at T_l = 25 h when the dilution ratio is everywhere below 0.05.

[101] To determine the value of τ we must first calculate the evolution of the fraction of mass within the plume (Figure A1, right). This is easily done in this example, but there is no difficulty to diagnose it from more sophisticated model integrations (i.e., 2D diffusion with shear or direct 3D LES simulations), as it simply requires the calculation of the integral of the mass of the tracer within the plume $M(t) = \frac{1}{V_p} \int_{V_p} \rho r \, dv$ (here $V_p = l_p$). Assuming that the mass evolution can be approximated by an exponential function,

$$M(t) = M(t_0) \exp(-t/\tau) \tag{A1}$$

having the same time integral than the exact mass evolution, yields an estimation of time τ,

$$\tau = \int_{t_0=0}^{+\infty} \exp(-t/\tau)\, dt = \frac{1}{M(t_0)} \int_{t_0=0}^{T_l} M(t)\, dt. \tag{A2}$$

For the simple case discussed here we found τ = 15.9 h.

[102] Figure A1 (right) shows the evolution of $M(t)/M(t_0)$ and $f(t)/M(t_0)$. The exponential function f approximates the M function within 20% for 80% of the mass evolution, with a tendency to underestimate the mass fractions at the beginning of the plume dissipation, and to overestimate it toward the end of the dissipation process.

[103] Similarly, the calculation of the value of K_{eff} for two reacting species A and B can be easily obtained for any plume simulation where chemistry is coupled to transport. Species A is assumed to have a background concentration $\overline{C_A}$ outside the plume, and species B is directly related to the emitted species (e.g., NO_x) and is found in large concentrations within the plume (see section 2.1.2). The species react with a rate constant K. In that configuration K_{eff} is computed from the following relation:

$$K_{eff} = \frac{\int_{t_0}^{T_l} \int_{l_p} K\, C_A\, C_B\, dl\, dt}{\overline{C_A} \int_{t_0}^{T_l} \int_{l_p} C_B\, dl\, dt}. \tag{A3}$$

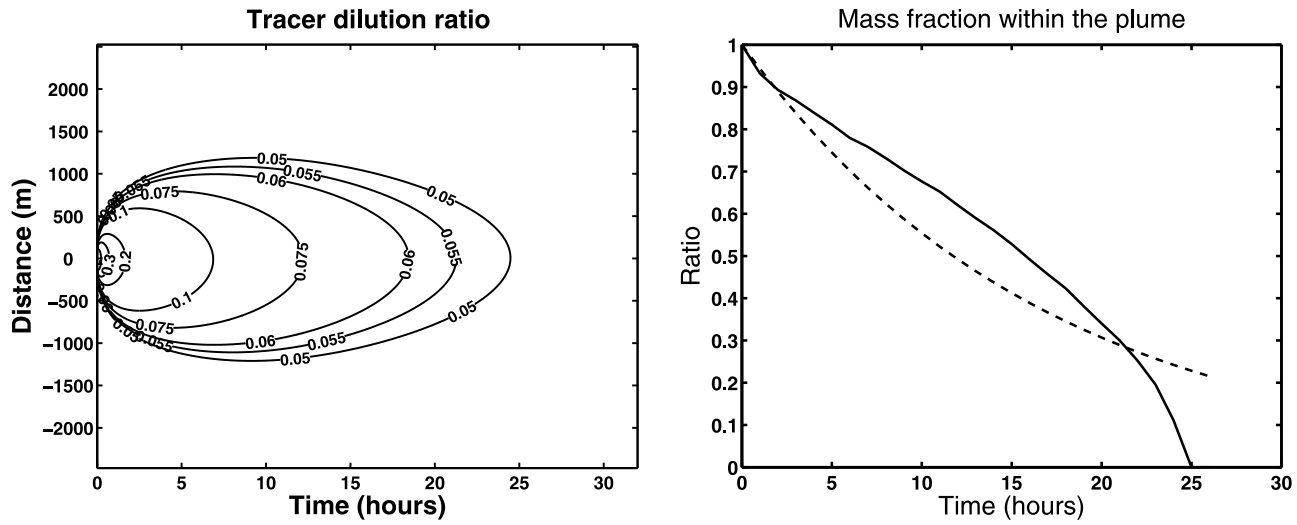

Figure A1. (left) Time evolution of a tracer normalized distribution due to the horizontal diffusion of a 250-m-wide plume. The isoline $r_l/r_p(t_0) = 0.05$ marks the evolution the plume boundary (see text). (right) Evolution of the normalized mass fraction within the plume (solid line) and its approximation by an exponential function (dotted line) having the same mass integral.

The integrals within this equation have to be evaluated inside the plume (within l_p) and up to the time T_l = 25 h after which $l_p = 0$.

[104] **Acknowledgments.** We thank D. Olivié for helpful comments on the manuscript. This work was supported by the European Union FP6 Integrated Project QUANTIFY (http://www.pa.op.dlr.de/quantify/), the French LEFE/CHAT INSU programme (http://www.insu.cnrs.fr) and the "Comité Aviation Atmosphère" of the DPAC programs. R. Paugam was supported by a grant from the fondation d'entreprise EADS.

References

Brasseur, G. P., J.-F. Müller, and C. Granier (1996), Atmospheric impact of NO_x by subsonic aircraft: A three-dimensional model study, *J. Geophys. Res.*, *101*, 1423–1428.

Brasseur, G. P., R. A. Cox, D. Hauglustaine, I. Isaksen, J. Lelieveld, D. H. Lister, R. Sausen, U. Schumann, A. Wahner, and P. Wiesen (1998), European scientific assessment of the atmospheric effects of aircraft emissions, *Atmos. Environ.*, *32*, 2329–2418.

Cariolle, D., and H. Teyssèdre (2007), A revised linear ozone photochemistry parameterization for use in transport and general circulation models: Multi-annual simulations, *Atmos. Chem. Phys.*, *7*, 2183–2196.

Cariolle, D., M. J. Evans, M. P. Chipperfield, N. Butkovskaya, A. Kukui, and G. Lebras (2008), Impact of the new HNO_3-forming channel of the HO_2+NO reaction on tropospheric HNO_3, NO_x, HO_x and ozone, *Atmos. Chem. Phys.*, *8*, 4061–4068.

Chosson, F., R. Paoli, and B. Cuenot (2008), Ship plume dispersion rates in convective boundary layer for chemistry models, *Atmos. Chem. Phys.*, *8*, 4841–4853.

Crutzen, P. (1974), Photochemical reactions initiated by and influencing ozone in unpolluted tropospheric air, *Tellus*, *26*, 47–57.

Dunkerton, T. (1978), On the mean meridional mass motions of the stratosphere and mesosphere, *J. Atmos. Sci.*, *53*, 2325–2333.

Durbeck, T., and T. Gerz (1996), Dispersion of aircraft exhausts in the free atmosphere, *J. Geophys. Res.*, *101*, 26,007–26,016.

Emanuel, K. A. (1991), A scheme for representing cumulus convection in large-scale models, *J. Atmos. Sci.*, *48*, 2313–2335.

Eyers, C. J., P. Norman, J. Middel, M. Plohr, K. Atkinson, and R. A. Christou (2004), AERO2k global aviation emissions inventories for 2002 and 2025, *Tech. Rep. QINETIQ/04/01113*, 144 pp., QinetiQ Lt., Farnborough, U. K. (Available at http://www.cate.mmu.ac.uk/reports_aero2k.asp?chg=projects&chg2+2)

Folberth, G. A., D. A. Hauglustaine, J. Lathière, and F. Brocheton (2006), Interactive chemistry in the Laboratoire de Météorologie Dynamique general circulation model: Model description and impact analysis of biogenic hydrocarbons on tropospheric chemistry, *Atmos. Chem. Phys.*, *6*, 2273–2319.

Garnier, F., C. Baudoin, P. Woods, and N. Louisnard (1997), Engine emission alteration in the near field of an aircraft, *Atmos. Environ.*, *31*, 1767–1781.

Gierens, K. M. (1996), Numerical simulations of persistent contrails, *J. Atmos. Sci.*, *53*, 3333–3348.

Gierens, K., U. Schumann, M. Helten, H. Smit, and P. H. Wang (2000), Ice-supersaturated regions and sub visible cirrus in the northern midlatitude upper troposphere, *J. Geophys. Res.*, *105*, 22,743–22,754.

Hauglustaine, D. A., F. Hourdin, L. Jourdain, M. A. Filiberti, S. Walters, J. F. Lamarque, and E. A. Holland (2004), Interactive chemistry in the Laboratoire de Météorologie Dynamique general circulation model: Description and background tropospheric chemistry evaluation, *J. Geophys. Res.*, *109*, D04314, doi:10.1029/2003JD003957.

Hourdin, F., and A. Armengaud (1999), The use of finite-volume methods for atmospheric advection of trace species: 1. Test of various formulations in a general circulation model, *Mon. Weather Rev.*, *127*, 822–837.

Kärcher, B. (1997), Heterogeneous chemistry in aircraft wakes: Constraints for uptake coefficients, *J. Geophys. Res.*, *102*, 19,119–19,135.

Kärcher, B., and S. K. Meilinger (1998), Perturbation of the aerosol layer by aviation-produced aerosols: A parameterization of plume processes, *Geophys. Res. Lett.*, *25*, 4465–4468.

Kärcher, B., M. M. Hirschberg, and P. Fabian (1996), Small-scale chemical evolutions of aircraft exhaust species at cruising altitudes, *J. Geophys. Res.*, *101*, 15,169–15,190.

Konopka, P. (1995), Analytical Gaussian solutions for anisotropic diffusion in a linear shear flow, *J. Non Equilib. Thermodyn.*, *20*, 78–91.

Kraabøl, A. G., T. K. Berntsen, J. K. Sundet, and F. Stordal (2002), Impacts of NO_x emissions from subsonic aircraft in a global three-dimensional chemistry transport model including plume processes, *J. Geophys. Res.*, *107*(D22), 4655, doi:10.1029/2001JD001019.

Lewellen, D. C., and W. S. Lewellen (2001), Effects of aircraft wake dynamics on measured and simulated NO_x and HO_x wake chemistry, *J. Geophys. Res.*, *102*, 19,119–19,135.

Meijer, E. W. (2001), Modeling the impact of subsonic aviation on the composition of the atmosphere, Ph. D. thesis, Tech. Univ. Eindhoven, Eindhoven, Netherlands.

Meilinger, S. K., B. Kärcher, and T. Peter (2005), Microphysics and heterogeneous chemistry in aircraft plumes—High sensitivity on local meteorology and atmospheric composition, *Atmos. Chem. Phys.*, *5*, 533–545.

Paoli, R., X. Vancassel, F. Garnier, and P. Mirabel (2008), Large-eddy simulation of a turbulent jet and a vortex sheet interaction: Particle formation and evolution in the near field of an aircraft wake, *Meteorol. Z.*, *17*, 131–144.

Paugam, R. (2008), Simulation numérique de l'évolution d'une traînée de condensation et de son interaction avec la turbulence atmosphérique, Ph.D. thesis, 211 pp., Ecole Centrale Paris, Châtenay Malabry, France.

Petry, H., J. Hendricks, M. Müllhoff, E. Lippert, A. Meier, and A. Ebel (1998), Chemical conversion of subsonic aircraft emissions in the dispersing plume: Calculation of effective emission indices, *J. Geophys. Res.*, *103*, 5759–5772.

Prather, M. J. (1986), Numerical advection by conservation of second order moments, *J. Geophys. Res.*, *91*, 6671–6681.

Sander, S. P., et al. (2006), Chemical kinetics and photochemical data for use in atmospheric studies: Evaluation 15, *JPL Publ., 06-2*, 523 pp.

Schlager, H., R. Baumann, M. Lichtenstern, A. Petzold, F. Arnold, M. Speidel, C. Gurk, and H. Fischer (2006), Aircraft-based trace gas measurements in a primary European ship corridor, in *Proceedings of the International Conference on Transport, Atmosphere and Climate (TAC)*, edited by R. Sausen et al., pp. 83–88, Eur. Comm., Oxford, U. K.

Schumann, U., P. Konopka, R. Baumann, B. Busen, T. Gerz, H. Schlager, P. Schulte, and H. Volkert (1995), Estimation of diffusion parameters of aircraft exhaust plumes near the tropopause from nitric oxide measurements and turbulence measurements, *J. Geophys.Res.*, *100*, 14,147–14,162.

Schumann, U., H. Schlager, F. Arnold, R. Baumann, P. Haschberger, and O. Klemm (1998), Dilution of aircraft exhaust plumes at cruise altitudes, *Atmos. Environ.*, *32*, 3097–3103.

Spinhirne, J. D., W. D. Hart, and D. P. Duda (1998), Evolution of the morphology and microphysics of contrail cirrus from airborne remote sensing, *Geophys. Res. Lett.*, *25*, 1153–1156.

Tompkins, A. M., K. Gierens, and G. Radel (2007), Ice supersaturation in the ECMWF integrated forcast system, *Q. J. R. Meteorol. Soc.*, *133*, 53–63.

van Leer, B. (1977), Towards the ultimate conservative difference scheme. Part IV: A new approach to numerical convection, *J. Comput. Phys.*, *23*, 276–299.

Vila-Guerau de Arellano, J., P. G. Duynkerke, P. J. Jonker, and P. J. H. Builtjes (1993), An observational study of the effects of time and space averaging in photochemical models, *Atmos. Environ.*, *27*, 353–362.

D. Cariolle, B. Cuénot, R. Paoli, and R. Paugam, CERFACS, URA1875, CNRS, 42 avenue Coriolis, F-31057 Toulouse, France. (daniel.cariolle@cerfacs.fr)

D. Caro, A. Cozic, and D. A. Hauglustaine, Laboratoire des Sciences du Climat et de l'Environnement, CEA, F-91191 Gif-sur-Yvette, France.